A MULTISCALE FINITE ELEMENT FAILURE MODEL FOR ANALYSIS OF THIN HETEROGENEOUS PLATES

By

Ghanshyam Pal

Thesis

Submitted to the Faculty of the

Graduate School of Vanderbilt University

in partial fulfillment of the requirements

for the degree of

MASTER OF SCIENCE

Civil Engineering

December 2008

Nashville, Tennessee

Approved By:

Dr. Caglar Oskay

Dr. Prodyot Basu

DEDICATION

This thesis is dedicated to my parents (Mr. B.R. Pal and Mrs. Ketki Pal) and my Family for putting their never ending emotional support and always showing me the righteous path and to my Teachers, for they are, who bestowed me with the knowledge I possess today.

ACKNOWLEDGMENTS

I would like to express my sincere thanks to the almighty, my parents and my family, whose blessings have always been guiding light to me. I am deeply thankful to my graduate advisor Dr. Caglar Oskay whose guidance, support and encouragement helped me all the times during research and writing of this thesis. At the same time, I am highly obliged to Dr. Prodyot K Basu for his help and instructive suggestions. I would also like to thank Dr. David Kosson, Chair, Department of Civil and Environmental Engineering for providing me the opportunity of graduate studies at Vanderbilt University. Last but not the least, I would like to thank my friends and well wishers at Vanderbilt University who have made my stay here a pleasant and memorable experience, so far.

TABLE OF CONTENTS

LIST OF TABLES

Table Page

LIST OF FIGURES

Figure Page

CHAPTER I

INTRODUCTION AND LITERATURE REVIEW

1.1 Motivation

Energy conservation and community security are the two main contemporary concerns. Seriousness of both the issues has captured attention of the modern engineering and scientific communities. These challenges are being responded enthusiastically by developing more energy efficient systems, alternate energy sources and novel high performance, tailored and light weight complex composite materials and alloy systems for specific applications in security and safety, energy, aerospace, biomedical, electronics and automotive sectors. However, economics of the development process and the underlying complexity of evolved systems restrict the use of expensive and time consuming physical testing to limited number of cases only. Recent advancements in computing power has made numerical simulation the third pillar of science after theory and experimentation, the other two pillars. A complete survey of the contemporary challenges in computational mechanics and composite materials can be found in [1].

Due to application specific properties and high strength to weight ratio (specially in polymer matrix composites), composite materials (metal, ceramic or polymer matrix composites) are becoming increasingly popular in industrial applications. Composite sections are increasingly being used to construct major proportion of primary structural members in civil, mechanical, aerospace and automobile industries.

Composite plane "$A380$" from Airbus Industries and "Dreamliner 787" from Boeing Co. are added new success stories for composite materials, as shown in Fig. 1.1.

Amongst the various possibilities, the use of plate like composites structural elements is quite extensive others. Today, composite thin plates are being used in a variety of applications such as manufacturing car and aeroplane body parts, retrofitting plates for civil structures, body armors, heat resisting tiles for spaceships, etc.

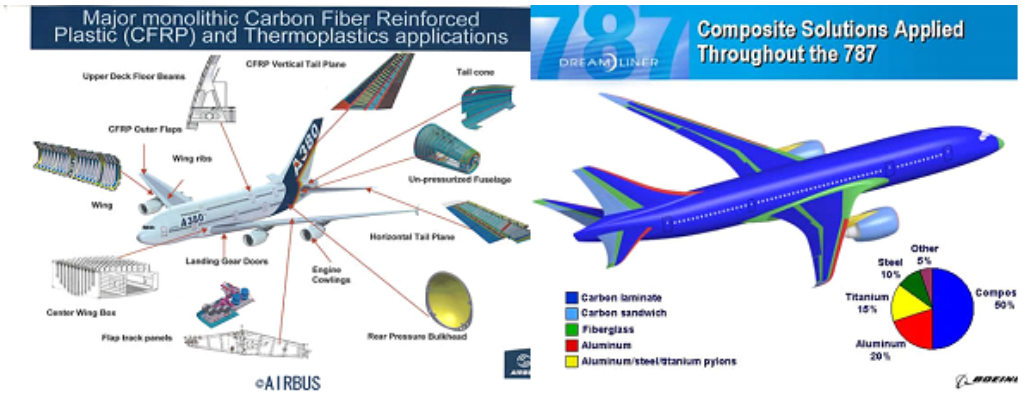

Figure 1.1. Composite planes from Airbus and Boeing (Source: http://www.carbonfiber.gr.jp)

1.2 Thin Plates

Technically, a plate is called thin if the characteristic wavelength of a deformation pattern is much longer than the plate thickness [2]. On the other hand a plate is viewed as a thick plate if this wave length is comparable to the plate thickness. Plates of intermediate thickness are called moderately thick plates. As a rule of thumb, if the ratio of thickness and the smaller span length of a plate is less than 1/20, it is treated as a thin plate. Problems associated with small deflections in isotropic, homogeneous

and elastic thin plates are solved via classical plate theory (CPT) of bending, which is based on Kirchhoff hypothesis.

In the case of thin elastic plates, if (u,v) are in-plane deformations along ($\mathbf{x} = x_1, x_2$) axes, respectively and w is transverse deflection (in x_3 direction), then the displacement field in CPT is given in accordance with Kirchhoff's hypotheses as following [3].

$$u(\mathbf{x}, x_3, t) = u_0(\mathbf{x}, t) - x_3 \frac{\partial w_0}{\partial x_1} \tag{1.1a}$$

$$v(\mathbf{x}, x_3, t) = v_0(\mathbf{x}, t) - x_3 \frac{\partial w_0}{\partial x_2} \tag{1.1b}$$

$$w(\mathbf{x}, x_3, t) = w_0(\mathbf{x}, t) \tag{1.1c}$$

where, $u_0(\mathbf{x}, t)$, $v_0(\mathbf{x}, t)$ and $w_0(\mathbf{x}, t)$ are the reference plane (or mid plane) displacements in their respective coordinate directions.

CPT plays a pivotal role in developing theories for thin heterogeneous plates. However, in case of composite plates the response (displacement) field is described using equivalent single layer (ESL) theory or layer-wise (LW) theory [3]. The ESL theory converts a three-dimensional problem into a two-dimensional problem by making suitable assumption about the displacement variation through the thickness. CPT is not directly applicable to modeling of composite thin plates but it has its counterpart called "classical laminated plate theory (CLPT)" in the realm of ESL theories for thin composite plates problems. Particularly, in the case of thin composite composite plates, ESL theory offers considerably accurate global behavior by a relatively simple approach.

ESL plate theories fail to capture an accurate assessment of displacement/stress field in the localized region of ply interface in laminated plates due to assumed continuity of displacements through the thickness. On the other hand, LW theories assume C^0 continuity of displacement field through laminate thickness. Thus, although the displacement is continuous across the ply in a laminate through the thickness, but possible discontinuity in the displacement derivative with respect to thickness allows the possibility of discontinuous transverse stresses at the interface of dissimilar laminae. With this advantage over ESL theories, LW theories are more suitable for describing various secondary or lamina level phenomenon such as delamination, matrix cracking, adhesive joint failure, resultant laminate strength after progressive ply failure, zig-zag behavior of in-plane displacements through the thickness, etc. However, LW plate theories give satisfactory results only for moderately thick or thick laminates as their direct application to thin plates yields spurious transverse stiffness which in turn violates Kirchhoff hypothesis of zero transverse deformation [3]. However, LW theories with selective or reduced integration for transverse shear terms model thin plate behavior with reasonable accuracy. An excellent review of capabilities of ESL and LW plate theories has been presented in [4].

1.3 Asymptotic Analysis

For almost all the composite materials, microstructure is periodic in nature, which results in the local response fields that are also periodic on microscopic scale. Therefore, for every composites, including the ones with randomly oriented reinforcement (composites with chopped fiber or whiskers as reinforcement), a microstructural repeating unit, called as "representative volume element (RVE)" can be deduced to represent the microscopic morphology of the composite system. But since RVE

dimensions are much smaller than the macroscopic dimensions, the entire coupled "macroscopic - microscopic" problem becomes intractable even by numerical methods. The solution to this intractability exists in the form of two-scale asymptotic analysis method which, essentially, separates the local analysis within the periodicity cell from the global or macroscopic analysis [5], [6]. The general assumed form of the solution in two scale asymptotic analysis is given as following.

$$u_i^{\zeta}(\mathbf{x},t) = u_i^0(\mathbf{x},t) + \sum_{\eta=1}^{\infty} \eta^{\zeta} u_i^{\zeta}(x,\mathbf{y},t) \tag{1.2}$$

The higher order terms e.g., u_1^{η}, u_2^{η} etc., in the above asymptotic series, are determined from the solutions of the local problems of various order of ζ. ζ is called as scaling factor, which is generally the ratio of macroscopic scale to microscopic scale associated with RVE.

The asymptotic analysis approach has been successfully applied by various authors in dealing with the elastic analysis of plates by [[7] - [11]]. In case of plates, the oscillatory nature of response fields depend upon three characteristic spatial scale: macroscopic scale, $\mathbf{x} := \{x, x_3\}$, where $x = \{x_1, x_2\}$, associated with the overall dimensions of the microstructure and two microscopic scales associated with the rescaled unit cell denoted by $y = \{y_1, y_2\}$, where $y = x/\zeta$, and $z = x_3/\epsilon$, associated with in-plane heteroginity and thickness, respectively. Two scaling constants, $0 < \zeta, \epsilon \ll 1$, respectively define the ratio between the characteristic planar dimension and thickness of the RVE with respect to the deformation wavelength at the macroscopic scale. Both of these scaling parameters the final plate constitutive equations. Caillarie [7] presented homogenization analysis of elastic and periodic thin heterogeneous plates with constant thickness for three different cases. In first case, homogenization ($\zeta \to 0$) of the plate problem succeeds the transformation of three dimensional problem to a

two dimensional problem ($\epsilon \rightarrow 0$). In the second case, ζ and ϵ are of same order whereas in third case, first ($\epsilon \rightarrow 0$), and then ($\zeta \rightarrow 0$). Kohn et al [8] carried out asymptotic analysis of bending of thin plate with varying thickness. In a series of three articles, [[9] - [11]] presented the approach to compute the effective moduli for thin heterogeneous plates with various geometric symmetries and thickness. In the second part of the series [10], author dealt with thin plates with geometrical symmetries where the three dimensional unit cell of thin plate is also symmetric. The last article of the series, [9], showed that in case of thin periodic plate where shape of the RVE is also a plate, the solution of the local unit cell problem can be approximated by one of the established plate theories depending upon the case. All these results presented in this series, along with many others, are provided in the form of a monograph by [12].

1.4 Continuum Damage Mechanics

Physically, a gradual loss stiffness and strength is resulted due to time dependent irreversible change in material's microstructure. Modeling of gradual evolution of this irreversible rearrangement of the microstructural geometry, of the possible inelastic deformation of multiply connected solids and of the resulting change in overall response are the challenges which are dealt under damage mechanics [18].

Damage in composite materials occurs in the form of different multiple-cracking modes, e.g. matrix cracking, matrix fiber interface cracking, delamination, fiber breaking etc. Lammerant et al [13] and Garg [14] modeled delamination in composite materials based on fracture mechanics approach coupled with a strain based criteria to initiate the damage. Godoy [15] used perturbation analysis to model damage in plates and shells. Voyiadjis [16] applied micromehanical damage mechanics to

study anisotropic damage in fiber reinforced metal matrix composites. They used a fourth order damage effect tensor for damage progression which is based on a second order damage tensor. Recently, Tay et al [17] proposed a method called "element failure method" based various strength of materials failure criterion to describe damage and progressive failure in composite materials.

Practically speaking, in composite materials, there is no isolated single crack that dominates the development of damage [19]. Due to complex crack pattern involving multiple damage modes, the formulation of damage problem based on individual crack mode becomes difficult to track. The alternative approach to study such a problem suggests to smear the effect of multiple crack mode into a locally homogeneous field and then take the smeared field quantities to characterize the damage state [19], [20], [21]. The approach is defined as continuum damage mechanics (CDM).

The theory of continuum damage was first introduced by Kachanov [20], [21], [22] using the concept of effective stress. The concept of effective stress compares the current damaged state of the materials against a fictitious undamaged state of the same material. The associated damage variable, based on effective stress concept, represents average material degradation accounting for various types of damages accruing at microscale level.

The loss of stiffness and hence structural integrity can be modeled using deterministic damage parameter(s). The associated damage parameter is an internal variable of the material system and it can be represented by a scalar, vector or tensor, complexity of microstructure and failure modes. Since damage parameter is an internal variable, therefore essentially the rate of the effective stiffness (and hence, stress) does not measure the damage evolution itself but it is a measurement of the effect of microcracking on the macro response [20], [21].

This approach of damage modeling has been applied by [23] for composite laminate where damage parameter is in vector form with five components, each representing a different lamina damage mode. A similar approach has been employed by Laedevze [24], Corigliano [25] and Collombert et al [26] to study the laminated composite structures.

1.5 Transformation Field Analysis

The presence of damage introduces eigenstrains in the composite system. In contrast to homogeneous materials, complex eigenstrain fields may be generated in the heterogeneous material system by one or more of these sources even under uniform overall stress, strain or temperature change [27], [28]. The influence of these transformation field on overall behavior and structural integrity of composite materials may well exceed that of mechanical loads.

In fact, these transformation fields may be considered as additional strains and stresses applied to the elastic composite aggregate, in superposition with overall stress or strain [27], [28]. In order to describe local transformation fields, the RVE is subdivided into sub-volumes or local volumes, each of which contains individual phases or portion of individual phases. If finite element analysis is used for the evaluation of local fields, then each element contains a portion of a constituent phase. Under the assumption that each sub-volume has uniform eigenstrain, the RVE volume average of local transformation fields can be calculated as the summation of sub-volume eigenstrain and the corresponding transformation influence function [29].

1.6 Proposed Methodology

Successful implementation of composite plates in critical real world applications demands a sound theoretical framework which can be used to predict the material response and failure under general loading conditions.

Consider a thin plate composed of a heterogeneous composite material system. Assumption of thin plates implies that the in-plane stresses are much greater than the other stress components. Assume that plate microstructure is periodic in two orthogonal directions, perpendicular to plate thickness.

In order to derive these periodic response fields, a set of boundary value problems (BVP) are developed for the plate unit cell by assuming that the kinematic response field can be represented by an asymptotic series with respect to scaling parameter(s). However, in order to make solution for the unit cell more tractable, the small unit cell along with the boundary conditions is rescaled with the help of scaling parameters.

The presence of damage causes in-elastic strains in the system. Transformation field analysis (TFA) is used to separate the total strain into elastic and in-elastic components. As a consequence of this separation, local problems are also separated into elastic influence function (EIF) problems and damage influence function (DIF) problems. A unique solution for these rescaled boundary value problems exists under the assumption that the applied forces, tractions and body force are sufficiently smooth and the domain boundaries are regular. The EIF and DIF problems are solved using finite element analysis. A static partitioning strategy has been adopted to create a reduced order model for unit cell problems. The phase average of the influence functions over the unit cell and various partitions with local stiffness tensor yields various coefficient tensors, which help in defining the constitutive behavior of

the macroscopic plate problem. This macroscopic thin plate problem is solved using a commercially available finite element code, namely, Abaqus. In this manuscript a rate-dependent model is used to characterize the evolution of damage within the microstructure. A Perzyna-type viscoplastic regularization [30], [31] of classical rate independent models [32] is used to alleviate the mesh dependence of the solution.

CHAPTER II

PROBLEM FORMULATION

2.1 Assumptions

The work presented in this chapter consists of formulation of the microscopic boundary value problems (BVP) associated with the asymptotic analysis of failure of thin plates. Before proceeding any further, it is imperative to list down all the assumptions of the formulation as follows.

1. The macrostructure involved in the problem is a thin plate. The constitutive relations for thin plates are discussed in Sec. 1.2.
2. The thin plate has periodic microstructure along the in-plane plate dimensions, i.e. the plate microstructure is composed of the periodic arrangement of a microscopic structural unit, termed as representative volume element (RVE).
3. The ratio of the planar dimension and thickness of RVE with respect to the deformation wavelength at macroscopic scale is defined by two scaling parameters ζ and ϵ such that $0 < \zeta, \epsilon \ll 1$. In the present problem, it is further assumed that the thickness and planar dimension of RVE are of same order, i.e $\epsilon = O(\zeta)$. Therefore, in the proposed asymptotic analysis hereunder, when $\epsilon \to 0, \zeta \to 0$, which means that the asymptotic expansion of the response fields for macroscopic problem can be expressed with the help of only one of the two scaling parameters.

4. The microscopic constituents of the microstructure are perfectly bonded together through interfaces.
5. The response fields are oscillatory in nature due to the presence of heterogeneities (as explained previous chapter). The heterogeneity in the microconstituents properties leads to an oscillatory response, characterized by the presence of three length scales: macroscopic scale, $\mathbf{x} := \{x, x_3\}$, where $x = \{x_1, x_2\}$, associated with the overall dimensions of the microstructure and two microscopic scales associated with the rescaled unit cell denoted by $y = \{y_1, y_2\}$, where $y = x/\zeta$, and $z = x_3/\epsilon$, associated with in-plane heteroginity and thickness, respectively. This oscillatory response can be represented using a two-scale decomposition of the coordinate vector:

$$f^{\zeta\epsilon}(\mathbf{x}) = f(x, \mathbf{y}(\mathbf{x})) \tag{2.1}$$

where, f denotes macroscopic response fields.
6. All the response fields are assumed to be periodic in microscopic planar directions, i.e. if $f(x, y, z)$ is any response field, $\hat{y}$ is the period of microstructure and k is a diagonal matrix with constant integer components then,

$$f(x, y, z) = f(x, y + k\hat{y}, z) \tag{2.2}$$

7. Due to involvement of multiple spatial scales, the partial derivative of a response is given by the following chain rule formula:

$$f^{\zeta\epsilon}_{,i} = \delta_{i\alpha}\left(f_{,x_\alpha} + \frac{1}{\zeta}f_{,y_\alpha}\right) + \delta_{i3}\frac{1}{\epsilon}f_{,z} \tag{2.3}$$

in which, a comma followed by an index denotes derivative with respect to the components of the position vector; a comma followed by a subscript variable x_α or y_i denotes a partial derivative with respect to the components of the macroscopic and microscopic position vectors, respectively; and δ_{ij} is the Kronecker delta.

8. The term $u_{(i,x_j)}$ for any response field is defined as following

$$u_{(i,x_j)} = \frac{\partial u_i}{\partial x_j} + \frac{\partial u_j}{\partial x_i} \tag{2.4}$$

9. The response fields superscripted by scaling parameter (ζ or ϵ) indicate that the macroscopic response field depends upon microstructural inhomogeneities.

10. L^{ζ}_{ijkl}, the tensor of elastic moduli, obeys the conditions of symmetry

$$L^{\zeta}_{ijkl} = L^{\zeta}_{jikl} = L^{\zeta}_{ijlk} = L^{\zeta}_{klij} \tag{2.5}$$

and positivity

$$\exists C_0 > 0; \quad L^{\zeta}_{ijkl}\xi_{ij}\xi_{kl} \geq C_0\xi_{ij}\xi_{kl} \quad \forall \xi_{ij} = \xi_{ji} \tag{2.6}$$

11. Throughout the manuscript, the greek subscripits have values of 1 and 2, whereas roman subscripits have values of 1, 2 and 3.

2.2 Definition of Problem

The problem definition starts with the fixing the domain of the thin plate macrostructure on macroscopic scale and that of the associated RVE on microscopic scale.

Domain of Heterogeneous Body

The domain of the heterogeneous body is defined as follows (Refer to Fig. 2.1):

$$\mathcal{B} := \left\{ \mathbf{x} \,|\, \mathbf{x} = (x, x_3),\, x = \{x_1,\, x_2\} \in \Omega,\, c_-^{\zeta}(x) \leq x_3 \leq c_+^{\zeta}(x) \right\} \tag{2.7}$$

in which, $\Omega \in \mathbb{R}^2$ is the reference surface parameterized by the Cartesian coordinate vector, x; x_3-axis denotes thickness direction; $\mathbf{x} = \{x_1,\, x_2,\, x_3\}$; $c_{\pm}^{\zeta}$ define the top $(+)$ and bottom $(-)$ boundaries of the body. Superscript ζ indicates dependence of the corresponding field on the planar heterogeneity.

Domain of RVE

The RVE, $\mathcal{Y}$, is defined in terms of the microscopic coordinates:

$$\mathcal{Y} := \left\{ \mathbf{y} \,|\, \mathbf{y} = (y, z),\, y = \{y_1,\, y_2\} \in Y,\, c^-(y) \leq z \leq c^+(y) \right\} \tag{2.8}$$

in which $Y \in \mathbb{R}^2$ is the reference surface in the RVE.

The boundaries of the RVE are defined as:

$$\Gamma_{\pm}^{\mathcal{Y}} = \left\{ \mathbf{y} \,|\, y \in Y,\, z = c^{\pm}(y) \right\} \tag{2.9a}$$

$$\Gamma_{\text{per}}^{\mathcal{Y}} = \left\{ \mathbf{y} \,|\, y \in \partial Y,\, c^-(y) < z < c^+(y) \right\} \tag{2.9b}$$

The boundary functions, $c^{\pm}$ are scaled with respect to the corresponding functions in the original single scale coordinate system: $c_{\pm}^{\zeta}(x) = \epsilon c^{\pm}(y)$.

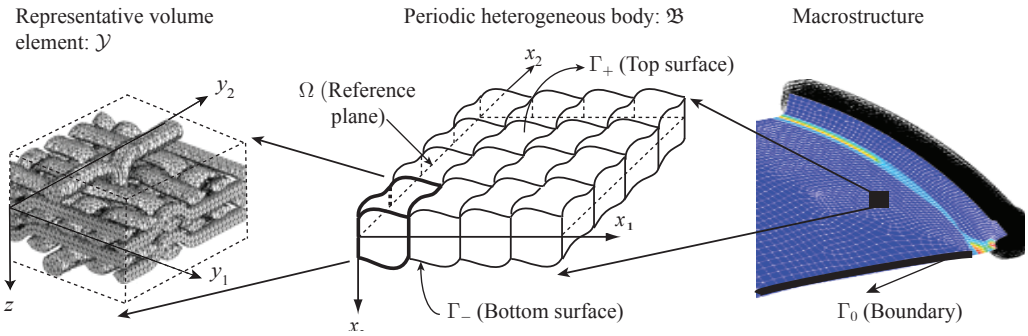

Figure 2.1. Macro- and microscopic structures.

2.3 Boundary Value Problem for Thin Composite Plates Failure Analysis

The following set of equations describes the boundary value problem associated with the failure of the heterogeneous body, where $\mathbf{x} \in \mathcal{B}$ and $t \in [0, t_0]$.

Equilibrium Equation

$$\sigma_{ij,j}^{\zeta}(\mathbf{x},t) + b_i^{\zeta}(\mathbf{x},t) = \rho^{\zeta}(\mathbf{x})\,\ddot{u}_i^{\zeta}(\mathbf{x},t) \tag{2.10}$$

Constitutive Equations

$$\sigma_{ij}^{\zeta}(\mathbf{x},t) = L_{ijkl}^{\zeta}(\mathbf{x})\left[\epsilon_{kl}^{\zeta}(\mathbf{x},t) - \mu_{kl}^{\zeta}(\mathbf{x},t)\right] \tag{2.11}$$

$$\mu_{ij}^{\zeta}(\mathbf{x},t) = \omega^{\zeta}(\mathbf{x},t)\,\epsilon_{ij}^{\zeta}(\mathbf{x},t) \tag{2.12}$$

Kinematic Equations

$$\epsilon_{ij}^{\zeta}(\mathbf{x},t) = \frac{1}{2}u_{(i,x_j)}^{\zeta}(\mathbf{x},t) \equiv \frac{1}{2}\left(\frac{\partial u_i^{\zeta}}{\partial x_j}+\frac{\partial u_j^{\zeta}}{\partial x_i}\right) \tag{2.13}$$

$$\omega^{\zeta}(\mathbf{x},t) = \omega^{\zeta}\left(\sigma_{ij}^{\zeta},\epsilon_{ij}^{\zeta},\mathbf{s}^{\zeta}\right) \tag{2.14}$$

where, u_i^{ζ} denotes the components of the displacement vector; σ_{ij}^{ζ} the Cauchy stress; ϵ_{ij}^{ζ} and μ_{ij}^{ζ} the total strain and inelastic strain tensors, respectively; $\omega^{\zeta} \in [0,1]$ is the scalar damage variable, with $\omega^{\zeta}=0$ corresponding to the state of no damage, and $\omega^{\zeta}=1$ denoting a complete loss of load carrying capacity; b_i^{ζ} the body force; $\rho^{\zeta}(\mathbf{x},t)$ the density, and; t the temporal coordinate. Superposed single and double dot correspond to temporal derivatives of order one and two, respectively.

Boundary Conditions

The boundary of the structure is defined by $\Gamma = \Gamma_{\pm} \cup \Gamma_0$, as illustrated in Fig. 2.1.

$$\Gamma_{\pm} = \left\{\mathbf{x}\,|\,x\in\Omega,\, x_3 = c_{\pm}^{\zeta}(\mathbf{x})\right\} \tag{2.15}$$

$$\Gamma_0 = \left\{\mathbf{x}\,|\,x\in\partial\Omega,\, c_{-}^{\zeta}(\mathbf{x}) < x_3 < c_{+}^{\zeta}(\mathbf{x})\right\} \tag{2.16}$$

The plate is assumed to be clamped along its side edge which leads to homogeneous displacement conditions on Γ_0, whereas traction boundary conditions are assumed on $\Gamma_{\pm}$:

$$u_i^{\zeta}(\mathbf{x},t) = 0 \quad ; \quad \mathbf{x}\in\Gamma_0; \quad t\in[0,t_{\mathrm{o}}] \tag{2.17}$$

$$\sigma_{ij}^{\zeta}(\mathbf{x},t)\,n_j = \bar{\tau}_i^{\pm}(\mathbf{x},t) \quad ; \quad \mathbf{x}\in\Gamma_{\pm}; \quad t\in[0,t_{\mathrm{o}}] \tag{2.18}$$

Initial Conditions

The initial conditions are assumed to be a function of the macroscopic coordinates only. The initial conditions are given as following:

$$u_i^{\zeta}(\mathbf{x},t) = \hat{u}_i(\mathbf{x}); \quad \dot{u}_i^{\zeta}(\mathbf{x},t) = \hat{v}_i(\mathbf{x}); \quad \mathbf{x} \in \mathcal{B}; \quad t = 0 \tag{2.19}$$

2.4 Homogenization of Thin Plates

Mathematical homogenization is a powerful analytical tool for the solution of problems in the mechanics of continuous media which are described by partial differential equation with rapidly oscillating coefficients. Homogenization with respect to local variables is employed to get the equation that describes the global behavior of the medium in terms of the slowly varying global variables / coefficients [6]. In the case of dynamic problem, time is an added variable both in local and global problems. Essentially, mathematical homogenization bridges the local solution with the global solution.

In the present approach, we start with the asymptotic expansion of the macroscopic displacements in the form suggested in [7] and [8]. Ref. [7] presents a detailed mathematical treatment of this type of displacement form for thin plates. Further, the concept of eigendeformation, suggested in [29] is employed in order to account for the inelastic fields appearing in the macroscopic system.

The asymptotic form for the generalized displacement fields for thin plates is given by the following equation.

$$u_i^{\zeta}(\mathbf{x},t) = \delta_{i3} w(x,t) + \zeta u_i^1(x,\mathbf{y},t) + \zeta^2 u_i^2(x,\mathbf{y},t) + ... \tag{2.20}$$

where, w is out of plane displacement and $u^1, u^2, ...$ demote higher order components of the total displacement. Using the kinematic relations given above as Eq. 2.13, the corresponding elastic strain fields can be given as:

$$\epsilon_{ij}^{\zeta}(\mathbf{x},t) = \sum_{\eta=0}^{\infty} \zeta^{\eta} \epsilon_{ij}^{\eta}(x,\mathbf{y},t) \tag{2.21}$$

where,

$$\epsilon_{\alpha\beta}^{0}(x,\mathbf{y},t) = u_{(\alpha,y_\beta)}^{1}; \quad \epsilon_{\alpha 3}^{0}(x,\mathbf{y},t) = \frac{1}{2} w_{,x_\alpha} + u_{(3,y_\alpha)}^{1}; \quad \epsilon_{33}^{0}(x,\mathbf{y},t) = u_{3,z}^{1}$$

$$\epsilon_{\alpha\beta}^{\eta}(x,\mathbf{y},t) = u_{(\alpha,x_\beta)}^{\eta} + u_{(\alpha,y_\beta)}^{\eta+1}; \quad \epsilon_{3\alpha}^{\eta}(x,\mathbf{y},t) = \frac{1}{2} u_{3,x_\alpha}^{\eta} + u_{(3,y_\alpha)}^{\eta+1}; \quad \epsilon_{33}^{1}(x,\mathbf{y},t) = u_{3,z}^{\eta+1}$$

$$\eta = 1, 2, \ldots$$

Due to asymptotic nature of strain fields, the associated stress field is also expressed in the asymptotic form, as given below.

$$\sigma_{ij}^{\zeta}(\mathbf{x},t) = \sum_{\eta=0}^{\infty} \zeta^{\eta} \sigma_{ij}^{\eta}(x,\mathbf{y},t) \tag{2.23}$$

where,

$$\sigma_{ij}^{\eta}(x,\mathbf{y},t) = L_{ijkl}(\mathbf{y}) \left[\epsilon_{kl}^{\eta}(x,\mathbf{y},t) - \mu_{kl}^{\eta}(x,\mathbf{y},t)\right] \tag{2.24}$$

$$\mu_{kl}^{\eta} = \omega(x,\mathbf{y},t) \epsilon_{ij}^{\eta}(x,\mathbf{y},t) \tag{2.25}$$

Finally, we need to rescale the load from macroscopic scale to microscopic scale. The scaling of the load has to be chosen in such a way that the flexural displacement of thin plates remain bounded as $\zeta \to 0$ during the homogenization process. The following set of equations represent the load rescaling used in this

research, as suggested in [12].

$$b_\alpha^\zeta(\mathbf{x},t) = \zeta b_\alpha(x,\mathbf{y},t) \quad ; \quad b_3^\zeta(\mathbf{x},t) = \zeta^2 b_3(x,\mathbf{y},t) \tag{2.26a}$$

$$\bar{\tau}_\alpha^\pm(\mathbf{x},t) = \zeta^2 \bar{p}_\alpha^\pm(x,t) \quad ; \quad \bar{\tau}_3^\pm(\mathbf{x},t) = \zeta^3 \bar{q}^\pm(x,t) \tag{2.26b}$$

$$\rho^\zeta(\mathbf{x}) = \rho(\mathbf{y}) \tag{2.26c}$$

The expressions for the corresponding stress and strain variables are plugged into Eq. 2.10. Next, the terms with the same power of ζ as coefficients are collected on both sides and equated. This yields individual equilibrium equations corresponding to various powers of ζ.

$$O(\zeta^{-1}) \;:\; \sigma^0_{ij,y_j} = 0 \tag{2.27a}$$

$$O(1) \;:\; \sigma^0_{i\alpha,x_\alpha} + \sigma^1_{ij,y_j} = 0 \tag{2.27b}$$

$$O(\zeta) \;:\; \sigma^1_{i\alpha,x_\alpha} + \sigma^2_{ij,y_j} + \delta_{i\alpha} b_\alpha = \delta_{i\alpha}\rho\ddot{u}^1_\alpha \tag{2.27c}$$

$$O(\zeta^2) \;:\; \sigma^2_{i\alpha,x_\alpha} + \sigma^3_{ij,y_j} + \delta_{i3} b_3 = \delta_{i\alpha}\rho\ddot{u}^2_\alpha + \delta_{3i}\rho\ddot{w} \tag{2.27d}$$

$$O(\zeta^\eta) \;:\; \sigma^\eta_{i\alpha,x_\alpha} + \sigma^{\eta+1}_{ij,y_j} = \delta_{i\alpha}\rho\ddot{u}^\eta_\alpha + \delta_{3i}\rho\ddot{u}^{\eta-2}_3, \quad \eta = 3,4,\ldots \tag{2.27e}$$

Now, after substituting displacement and stress decompositions (Eqs. 2.4 and 2.23) into Eqs. 2.17 and 2.18, and using Eq. 2.26b, the boundary conditions of various orders are obtained as below.

$$O(1) \;:\; \sigma^0_{ij}(x,\mathbf{y},t)n_j = 0, \quad x \in \Gamma_\pm; \qquad w(x,t) = 0, \quad x \in \Gamma_0 \tag{2.28a}$$

$$O(\zeta) \;:\; \sigma^1_{ij}(x,\mathbf{y},t)n_j = 0, \quad x \in \Gamma_\pm; \qquad u^1_i(x,\mathbf{y},t) = 0, \quad x \in \Gamma_0 \tag{2.28b}$$

$$\mathrm{O}(\zeta^2) : \sigma^2_{ij}(x,\mathbf{y},t)n_j = \delta_{i\alpha}\bar{\tau}^{\pm}_{\alpha}(x), \quad x \in \Gamma_{\pm}; \quad u^2_i(x,\mathbf{y},t) = 0, \quad x \in \Gamma_0 \text{(2.28c)}$$

$$\mathrm{O}(\zeta^3) : \sigma^3_{ij}(x,\mathbf{y},t)n_j = \delta_{i3}\bar{\tau}^{\pm}_{3}(x), \quad x \in \Gamma_{\pm}; \quad u^3_i(x,\mathbf{y},t) = 0, \quad x \in \Gamma_0 \text{(2.28d)}$$

$$\mathrm{O}(\zeta^\eta) : \sigma^\eta_{ij}(x,\mathbf{y},t)n_j = 0, \quad x \in \Gamma_{\pm}; \qquad u^\eta_i(x,\mathbf{y},t) = 0, \quad x \in \Gamma_0 \text{(2.28e)}$$

$$\eta = 4, 5, \ldots$$

2.5 First Order Microscale Problem

In order to develop microscopic problems of various order, the equilibrium equations presented in Sec. 2.4 are considered one by one, along with the corresponding boundary conditions. The first order microscopic problem is developed by considering $O(\zeta^{-1})$ (Eq. 2.27a) equilibrium equation and $O(1)$ (Eq. 2.28a) boundary condition. Substituting kinematic relations (Eq. 2.13) yields the final expression for the first order microscopic problem (**RVE^1**), as described below.

The First Order RVE problem (RVE^1)

***Given*:** material properties, $L_{ijkl}(\mathbf{y})$, macroscopic strains, $w_{,x_\alpha}$, and the inelastic strain field, μ^0_{kl}

***Find*:** For a fixed $\bar{x} \in \Omega$ and $\bar{t} \in [0, t_0]$, the microscopic deformations, $u^1_i(\bar{x}, \mathbf{y}, \bar{t}) \in \bar{\mathcal{Y}} \to \mathbb{R}$ which satisfy

***Equilibrium*:** Equilibrium condition is given below:

- $\left\{ L_{ijkl}(\mathbf{y})\, u^1_{(k,y_l)}(\bar{x},\mathbf{y},\bar{t}) + L_{ij\alpha 3}(\mathbf{y})\, w_{,x_\alpha}(\bar{x},\bar{t}) - L_{ijkl}(\mathbf{y})\, \mu^0_{kl}(\bar{x},\mathbf{y},\bar{t}) \right\}_{,y_j} = 0$

***Boundary Conditions*:** The boundary conditions are such that:

- $u^1_{(i,y_j)}$ periodic on $\mathbf{y} \in \Gamma^{\mathcal{Y}}_0$
- $\left\{ L_{ijkl} u^1_{(k,y_l)} + L_{ij\alpha 3} w_{,x_\alpha} - L_{ijkl}\mu^0_{kl} \right\} n_j = 0$ on $\mathbf{y} \in \Gamma^{\mathcal{Y}}_{\pm}$

The microscopic problem **RVE^1** can be solved with the help of the concept of transformation field analysis (Sec. 1.5) and eigendeformation for a given macroscopic state of the system. As the above displacement expression is valid for arbitrary damage state, therefore for a frozen system, i.e. at fixed time and fixed macroscopic state, the problem **RVE^1** can be separated into two linear systems. First, It is considered that the resulting system is damage free, i.e. $\mu^0_{kl} = 0 \rightarrow u^{1\mu}_i = 0$, So that only driving force left in the system is $w_{,x_\alpha}$. The corresponding displacement field is given by $u^{1w}_i(x, y, t)$. At this state, the microscopic problem **RVE^1** can be trivially satisfied by the following displacement field.

$$u^1_i = u^{1w}_i(x, \mathbf{y}, t) = u_i(x, t) - \hat{z}\delta_{i\alpha} w_{,x_\alpha}(x, t) \tag{2.29}$$

where, $\hat{z} = z - \langle z \rangle$, and; $\langle \cdot \rangle := 1/|\mathcal{Y}| \int_{\mathcal{Y}} \cdot d\mathcal{Y}$ denotes volume averaging on the RVE.

Next, consider that microscopic deformations vanish at arbitrary damage state and the only driving force left in the system is μ^0_{kl}. The displacement field in this case is denoted by $u^{1\mu}_i$. The resulting system of partial differential equations (PDE) can be solved using Green's function. The Green's function represents the solution of the PDE, when the original force function is replaced by Dirac's delta function [33]. Following the terminology proposed in [27] and [28], the resulting problem with dirac delta function is referred to as "First order damage influence function problem (**DIF^1**)" (as given below) and the corresponding solution is termed as "First order damage influence function, $\tilde{\Theta}_{ikl}$".

The First Order Damage Influence Function problem (DIF^1).

***Given*:** Material properties, $L_{ijmn}(\mathbf{y})$ and d is Dirac delta function.

***Find*:** $\tilde{\Theta}_{ikl}(\mathbf{y}, \hat{\mathbf{y}}) : \bar{\mathcal{Y}} \times \bar{\mathcal{Y}} \rightarrow \mathbb{R}$ such that:

***Equilibrium*:** Equilibrium condition as given below:

- $\left\{ L_{ijmn}\left(\mathbf{y}\right)\left(\tilde{\Theta}_{(m,y_n)kl}\left(\mathbf{y},\hat{\mathbf{y}}\right)+I_{mnkl}d\left(\mathbf{y}-\hat{\mathbf{y}}\right)\right)\right\}_{,y_j}=0;\quad \mathbf{y},\hat{\mathbf{y}}\in\mathcal{Y}$

Boundary conditions: The boundary conditions are such that:

- $\tilde{\Theta}_{ik\beta}$ periodic on $\mathbf{y}\in\Gamma_0^{\mathcal{Y}}$
- $L_{ijmn}\left(\mathbf{y}\right)\left(\tilde{\Theta}_{(m,y_n)kl}\left(\mathbf{y},\hat{\mathbf{y}}\right)+I_{mnkl}d\left(\mathbf{y}-\hat{\mathbf{y}}\right)\right)n_j=0$ on $\mathbf{y}\in\Gamma_{\pm}^{\mathcal{Y}}$

The displacement field in this case, $u_i^{1\mu}$ is obtained using the first order damage influence function , $\tilde{\Theta}_{ikl}$, as follows.

$$u_i^1=u_i^{1\mu}(x,\mathbf{y},t)=\int_{\mathcal{Y}}\tilde{\Theta}_{ikl}(\mathbf{y},\hat{\mathbf{y}})\mu_{kl}^o(x,\hat{\mathbf{y}},t)d\hat{\mathbf{y}} \tag{2.30}$$

The final expression for the overall displacement field, u_i^1, is given by joining the above two displacement fields, u_i^{1w} and $u_i^{1\mu}$ as follows.

$$u_i^1(x,\mathbf{y},t) = u_i^{1w}(x,\mathbf{y},t)+u_i^{1\mu}(x,\mathbf{y},t) \tag{2.31a}$$

$$u_i^1(x,\mathbf{y},t) = u_i(x,t)-\hat{z}\delta_{i\alpha}w_{,x_\alpha}(x,t)+\int_{\mathcal{Y}}\tilde{\Theta}_{ikl}(\mathbf{y},\hat{\mathbf{y}})\mu_{kl}^o(x,\hat{\mathbf{y}},t)d\hat{\mathbf{y}} \tag{2.31b}$$

The overall eigenstrain, μ_{ij}^0 in this case is given as follows.

$$\mu_{ij}^0(x,\mathbf{y},t)=\omega(x,\mathbf{y},t)\int_{\mathcal{Y}}\tilde{\Theta}_{(i,y_j)kl}(\mathbf{y},\hat{\mathbf{y}})\mu_{kl}^0(x,\hat{\mathbf{y}},t)d\hat{\mathbf{y}} \tag{2.32}$$

The above is a homogeneous integral equation. For an arbitrary damage state, ω, it can only be satisfied trivially [34], that is $\mu_{ij}^0=0$ and the first order displacement expression is given by Eq. (2.29).

2.6 Second Order Microscopic Problem

The $O(\zeta)$ equilibrium equation along with the $O(1)$ constitutive and kinematic equations, and initial and boundary conditions form the second order microscale problem (**RVE^2**) as summarized below.

The Second Order RVE problem (RVE^2).

***Given*:** Material properties, $L_{ijkl}(\mathbf{y})$, macroscopic strains, $w_{,x_\alpha x_\beta}$ and u_{i,x_α}, and inelastic strain tensor, μ_{kl}

***Find*:** For a fixed $\bar{x} \in \Omega$ and $\bar{t} \in [0, t_0]$, the microscopic displacements $u_i^2(\bar{x}, \mathbf{y}, \bar{t}) \in \bar{\mathcal{Y}} \to \mathbb{R}$ which satisfy

***Equilibrium*:** Equilibrium condition as given below:

- $\Big\{ L_{ijkl}(\mathbf{y})\, u^2_{(k,y_l)}(\bar{x}, \mathbf{y}, \bar{t}) + L_{ij\alpha 3}(\mathbf{y})\, u_{3,x_\alpha}(\bar{x}, \bar{t}) + L_{ij\alpha\beta}(\mathbf{y}) \times \big(u_{(\alpha,x_\beta)}(\bar{x}, t) - \hat{z} w_{,x_\alpha x_\beta}(\bar{x}, t) \big) - L_{ijkl}(\mathbf{y})\, \mu_{kl}(\bar{x}, \mathbf{y}, \bar{t}) \Big\}_{,y_j} = 0$

***Boundary Condition*:** The boundary conditions are such that:

- $u^2_{(i,y_j)}$ periodic on $\mathbf{y} \in \Gamma_0^{\mathcal{Y}}$
- $\Big\{ L_{ijkl}(\mathbf{y})\, u^2_{(k,y_l)}(\bar{x}, \mathbf{y}, \bar{t}) + L_{ij\alpha 3}(\mathbf{y})\, u_{3,x_\alpha}(\bar{x}, \bar{t}) + L_{ij\alpha\beta}(\mathbf{y}) \times \big(u_{(\alpha,x_\beta)}(\bar{x}, t) - \hat{z} w_{,x_\alpha x_\beta}(\bar{x}, t) \big) - L_{ijkl}(\mathbf{y})\, \mu_{kl}(\bar{x}, \mathbf{y}, \bar{t}) \Big\} n_j = 0$ on $\mathbf{y} \in \Gamma_{\pm}^{\mathcal{Y}}$

The second order microscale problem is evaluated analogous to the first order problem using the eigendeformation concept. The forcing terms in **RVE^2** are the macroscopic generalized strains, u_{i,x_α} and $w_{,x_\alpha}$ as well as the inelastic strains, $\mu_{ij}(x, \hat{\mathbf{y}}, t)$. The microscopic displacement field is evaluated by considering the following decomposition:

$$u_i^2 = u_i^{2w} + u_i^{2u} \tag{2.33}$$

in which, u_i^{2w} and u_i^{2u} correspond to the displacement components due to the forcing terms associated with the macroscopic displacements w and u_i, respectively. First, consider the case when $w = 0$. Employing the eigendeformation concept, the microscopic displacement field is expressed in terms of the influence functions:

$$u_i^{2u}(x, \mathbf{y}, t) = \Theta_{i\alpha\beta}(\mathbf{y})\, u_{(\alpha,x_\beta)}(x,t) - \hat{z}\delta_{i\alpha} u_{3,x_\alpha}(x,t) + \int_{\mathcal{Y}} \tilde{\Theta}_{ikl}(\mathbf{y}, \hat{\mathbf{y}}) \bar{\mu}_{kl}(x, \hat{\mathbf{y}}, t) d\hat{\mathbf{y}} \quad (2.34)$$

where, $\bar{\mu}_{kl}(x, \hat{\mathbf{y}}, t)$ denotes the components of the inelastic strain field due to in-plane deformations, and; $\Theta_{ik\beta}$ is the first order elastic influence function. $\Theta_{ik\beta}$ is the solution to the first order elastic influence function problem outlined below as **EIF²**.

The First Order Elastic Influence Function problem (EIF²).

***Given*:** Material properties $L_{ijkl}(\mathbf{y})$.

***Find*:** $\Theta_{i\alpha\beta}(\mathbf{y}) : \bar{\mathcal{Y}} \to \mathbb{R}$ such that:

***Equilibrium*:** Equilibrium condition as given below:

- $\left\{ L_{ijmn} \Theta_{(m,y_n)\alpha\beta}(\mathbf{y}) + L_{ij\alpha\beta}(\mathbf{y}) \right\}_{,y_j} = 0$

***Boundary Condition*:** The Boundary conditions are such that:

- $\Theta_{i\alpha\beta}$ periodic on $\mathbf{y} \in \Gamma_0^{\mathcal{Y}}$
- $L_{ijmn}(\mathbf{y}) \left(\Theta_{(m,y_n)\alpha\beta}(\mathbf{y}) + I_{mn\alpha\beta}(\mathbf{y}) \right) n_j = 0$ on $\mathbf{y} \in \Gamma_{\pm}^{\mathcal{Y}}$

Considering the case when $u_i = 0$ with nonzero w, the microscopic displacement field is expressed in terms of the second order influence functions as

$$u_i^{2w}(x, \mathbf{y}, t) = \Xi_{i\alpha\beta}(\mathbf{y})\, w_{,x_\alpha x_\beta}(x,t) + \int_{\mathcal{Y}} \tilde{\Xi}_{ikl}(\mathbf{y}, \hat{\mathbf{y}}) \hat{\mu}_{kl}(x, \hat{\mathbf{y}}, t) d\hat{\mathbf{y}} \quad (2.35)$$

where, $\hat{\mu}_{ij}$ denotes the components of the inelastic strain field due to the bending deformation; $\Xi_{i\alpha\beta}$ and $\tilde{\Xi}_{ikl}$ the second order elastic and damage influence functions,

respectively. $\Xi_{i\alpha\beta}$ and $\tilde{\Xi}_{ikl}$ are solutions to elastic and damage influence function problems ($\mathbf{EIF}^2$) and ($\mathbf{DIF}^2$), respectively, as summarized below. Under general loading conditions (nonzero u_i and w with arbitrary damage state, ω), microscopic displacement field, u_i^2 is given by Eq. 2.33 with the right hand side terms provided by Eqs. 2.34 and 2.35.

The Second Order Elastic Influence Function problem ($\mathbf{EIF^2}$).

***Given*:** Material properties $L_{ijkl}(\mathbf{y})$.

***Find*:** $\Xi_{i\alpha\beta}(\mathbf{y}) : \bar{\mathcal{Y}} \to \mathbb{R}$ such that:

***Equilibrium*:** Equilibrium condition as given below:

- $\left\{L_{ijmn}\Xi_{(m,y_n)\alpha\beta}(\mathbf{y}) - \hat{z}L_{ij\alpha\beta}(\mathbf{y})\right\}_{,y_j} = 0$

***Boundary Condition*:** The boundary conditions are such that:

- $\Xi_{i\alpha\beta}$ periodic on $\mathbf{y} \in \Gamma_0^{\mathcal{Y}}$
- $L_{ijmn}(\mathbf{y})\left(\Xi_{(m,y_n)\alpha\beta}(\mathbf{y}) - \hat{z}I_{mn\alpha\beta}(\mathbf{y})\right)n_j = 0$ on $\mathbf{y} \in \Gamma_{\pm}^{\mathcal{Y}}$

The Second Order Damage Influence Function problem ($\mathbf{DIF^2}$).

***Given*:** Material properties, $L_{ijmn}(\mathbf{y})$ and d is Dirac delta function.

***Find*:** $\tilde{\Xi}_{ikl}(\mathbf{y}, \hat{\mathbf{y}}) : \bar{\mathcal{Y}} \times \bar{\mathcal{Y}} \to \mathbb{R}$ such that:

***Equilibrium*:** Equilibrium condition as given below:

- $\left\{L_{ijmn}(\mathbf{y})\left(\tilde{\Xi}_{(m,y_n)kl}(\mathbf{y}, \hat{\mathbf{y}}) - \hat{z}I_{mnkl}d(\mathbf{y} - \hat{\mathbf{y}})\right)\right\}_{,y_j} = 0; \quad \mathbf{y}, \hat{\mathbf{y}} \in \mathcal{Y}$

***Boundary Condition*:** The boundary conditions are such that:

- $\tilde{\Xi}_{ik\beta}$ periodic on $\mathbf{y} \in \Gamma_0^{\mathcal{Y}}$
- $L_{ijmn}(\mathbf{y})\left(\tilde{\Xi}_{(m,y_n)kl}(\mathbf{y}, \hat{\mathbf{y}}) - \hat{z}I_{mnkl}d(\mathbf{y} - \hat{\mathbf{y}})\right)n_j = 0$ on $\mathbf{y} \in \Gamma_{\pm}^{\mathcal{Y}}$

2.7 Development of Macroscopic Constitutive Relations

Solution of microscopic elastic and in-elastic influence function problem (EIF^1, EIF^2, DIF^1 and DIF^2) completes the computation for $u^1(x,\mathbf{y},t)$ and $u^2(x,\mathbf{y},t)$. Then, using kinematic Eq. 2.22a, stress field σ^1_{ij} is given as following.

$$\sigma^1_{ij}(x,\mathbf{y},t) = L_{ijkl}\epsilon^1_{kl}(x,\mathbf{y},t) \tag{2.36}$$

$$\begin{aligned}\sigma^1_{(ij)}(x,\mathbf{y},t) = L_{ij\alpha\beta}\epsilon^1_{(\alpha\beta)}(x,\mathbf{y},t) + 2L_{ij3\beta}\epsilon^1_{(3\beta)}(x,\mathbf{y},t)\\ +L_{ij33}\epsilon^1_{(33)}(x,\mathbf{y},t)\end{aligned} \tag{2.37}$$

where,

$$\epsilon^1_{\alpha\beta}(x,\mathbf{y},t) = u^1_{(\alpha,x_\beta)}(x,\mathbf{y},t) + u^2_{(\alpha,y_\beta)}(x,\mathbf{y},t) \tag{2.38a}$$

$$\epsilon^1_{3\beta}(x,\mathbf{y},t) = \frac{1}{2}u^1_{3,x_\beta}(x,\mathbf{y},t) + u^2_{(3,y_\beta)}(x,\mathbf{y},t) \tag{2.38b}$$

$$\epsilon^1_{(33)}(x,\mathbf{y},t) = u^2_{(3,y_3)}(x,\mathbf{y},t) \tag{2.38c}$$

and,

$$u^1_{(\alpha,x_\beta)}(x,\mathbf{y},t) = u_{(\alpha,x_\beta)}(x,t) - \hat{z}w_{,x_\alpha x_\beta}(x,t) \tag{2.39a}$$

$$u^1_{3,x_i}(x,t) = u_{3,x_i}(x,t) \tag{2.39b}$$

$$u^2_{(i,y_j)\lambda\delta}(x,\mathbf{y},t) = \Theta_{(i,y_j)\lambda\delta}(x,\mathbf{y},t)\,u_{\lambda,x_\delta}(x,t)\,\Xi_{(i,y_j)\lambda\delta}(x,\mathbf{y},t)\,w_{,x_\lambda x_\delta}(x,t) \tag{2.39c}$$

After plugging the above mentioned strain expression in Eq. 2.23 and rearranging, stress field σ_{ij}^{1}, is given as following.

$$\begin{aligned}\sigma_{ij}^{1}\left(x,\mathbf{y},t\right) = L_{ijkl}\left(\mathbf{y}\right)A_{kl\alpha\beta}\left(\mathbf{y}\right)u_{\alpha,x_\beta}\left(x,t\right) - L_{ijkl}\left(\mathbf{y}\right)E_{kl\alpha\beta}\left(\mathbf{y}\right)\omega_{,x_\alpha x_\beta}\left(x,t\right)\\ +L_{ijkl}\left(\mathbf{y}\right)\int_{\mathcal{Y}}\tilde{A}_{klmn}\left(\mathbf{y},\hat{\mathbf{y}}\right)\bar{\mu}_{mn}\left(x,\hat{\mathbf{y}},t\right)d\hat{\mathbf{y}}\\ +L_{ijkl}\left(\mathbf{y}\right)\int_{\mathcal{Y}}\tilde{E}_{klmn}\left(\mathbf{y},\hat{\mathbf{y}}\right)\hat{\mu}_{mn}\left(x,\hat{\mathbf{y}},t\right)d\hat{\mathbf{y}}\end{aligned} \tag{2.40}$$

where,

$$A_{ij\alpha\beta}\left(\mathbf{y}\right) = I_{ij\alpha\beta} + \Theta_{(i,y_j)\alpha\beta}\left(\mathbf{y}\right) \tag{2.41}$$

$$E_{ij\alpha\beta}\left(\mathbf{y}\right) = I_{ij\alpha\beta} - \hat{z}\Xi_{(i,y_j)\alpha\beta}\left(\mathbf{y}\right) \tag{2.42}$$

$$\tilde{A}_{ijkl}\left(\mathbf{y},\hat{\mathbf{y}}\right) = \tilde{\Theta}_{(i,y_j)kl}\left(\mathbf{y},\hat{\mathbf{y}}\right) - d\left(\hat{\mathbf{y}}-\mathbf{y}\right)I_{ijkl} \tag{2.43}$$

$$\tilde{E}_{ijkl}\left(\mathbf{y},\hat{\mathbf{y}}\right) = \tilde{\Xi}_{(i,y_j)kl}\left(\mathbf{y},\hat{\mathbf{y}}\right) - d\left(\hat{\mathbf{y}}-\mathbf{y}\right)I_{ijkl} \tag{2.44}$$

It can be shown that for the given displacement field and stress field (Eq. 2.40), the transverse shear stress component vanishes [12], i.e.

$$\langle\sigma_{3j}^{1}\left(x,\mathbf{y},t\right)\rangle = 0 \tag{2.45}$$

Next, total force resultant $\mathcal{N}_{\alpha\beta}(x,t)$ and total moment resultant $\mathcal{M}_{\alpha\beta}$ (x, t) are defined as follows.

$$\mathcal{N}_{\alpha\beta}(x,t) = <\sigma_{\alpha\beta}^{1}> \tag{2.46}$$

$$\mathcal{M}_{\alpha\beta}(x,t) = <\hat{z}\sigma_{\alpha\beta}^{1}> \tag{2.47}$$

$$Q_\alpha(x,t) = \langle \sigma^2_{3\alpha} \rangle \tag{2.48}$$

$$e_{\alpha\beta}(x,t) = u_{\alpha,x_\beta}(x,t) \tag{2.49}$$

$$\kappa_{\alpha\beta}(x,t) = -w_{,x_\alpha x_\beta}(x,t) \tag{2.50}$$

In order to develop unit cell equilibrium equation for in-plane force resultant, the $O(\zeta)$ equilibrium equation is integrated over the unit cell and both sides of the equation are divided by the volume of the unit cell.

$$\frac{1}{\mathcal{Y}} \int_{\mathcal{Y}} [\sigma^1_{i\alpha,x_\alpha}(x,\mathbf{y},t) + \sigma^2_{ij,y_j}(x,\mathbf{y},t) + \delta_{i\alpha} b_\alpha(x,\mathbf{y},t)] dV = \frac{1}{\mathcal{Y}} \int_{\mathcal{Y}} [\delta_{i\alpha} \rho \ddot{u}^1_\alpha(x,\mathbf{y},t)] dV \tag{2.51}$$

Using the Gauss divergence theorem on the second term on left hand side and definition of in-plane force resultant $\mathcal{N}_{\alpha\beta}$, the following relationship is obtained.

$$\mathcal{N}_{\alpha\beta,x_\beta}(x,t) + \frac{1}{\mathcal{Y}} \int_Y \sigma^2_{ij} n_j(x,\mathbf{y},t)\, dY + \langle b_\alpha \rangle(x,t) = \langle \rho \rangle \ddot{u}_\alpha(x,t) - \langle \rho \hat{z} \rangle \ddot{w}_{,x_\alpha}(x,t) \tag{2.52}$$

Using $O(\zeta)^2$ unit cell boundary condition, the above Eq. 2.7 can be rewritten as follows.

$$\mathcal{N}_{\alpha\beta,x_\beta}(x,t) + q_\alpha(x,t) = \langle \rho \rangle \ddot{u}_\alpha(x,t) - \langle \rho \hat{z} \rangle \ddot{w}_{,x_\alpha}(x,t) \tag{2.53}$$

where, $q_\alpha(x,t)$ denotes the traction acting at the top and bottom surfaces of the plate as well as the body forces as given below.

$$q_\alpha(x,t) = \langle b_\alpha \rangle(x,t) + \langle G_+ \rangle_Y \bar{\tau}^+_\alpha(x,t) + \langle G_- \rangle_Y \bar{\tau}^-_\alpha(x,t) \tag{2.54}$$

and $\langle\cdot\rangle_Y = \int_Y \cdot dy$, and $G_\pm(y)$is the metric tensor which accounts for the arbitrary shape of the RVE boundaries, defined below.

$$G_\pm(y) = \sqrt{(1 + c_{,y_1}^{2\pm} + c_{,y_2}^{2\pm})} \tag{2.55}$$

Next, again Eq. 2.7 is pre-multiplied with $\hat{z}$ and averaged over the unit cell.

$$\frac{1}{\mathcal{Y}}\int_{\mathcal{Y}} \hat{z}[\sigma^1_{i\alpha,x_\alpha}(x,\mathbf{y},t) + \sigma^2_{ij,y_j}(x,\mathbf{y},t) + \delta_{i\alpha}b_\alpha(x,\mathbf{y},t)]dV = \frac{1}{\mathcal{Y}}\int_{\mathcal{Y}} \hat{z}[\delta_{i\alpha}\rho\ddot{u}^1_\alpha(x,\mathbf{y},t)]dV \tag{2.56}$$

Now, consider the second term on left hand side in the above equation.

$$\begin{aligned}\int_{\mathcal{Y}} \hat{z}\sigma^2_{ij,y_j}(x,\mathbf{y},t)\,dV &= \int_{\mathcal{Y}} [\hat{z}\sigma^2_{ij}(x,\mathbf{y},t)]_{,y_j}dV - \int_{\mathcal{Y}} \hat{z}_{,y_j}\sigma^2_{ij}(x,\mathbf{y},t)\,dV \\ &= \int_Y \hat{z}\sigma^2_{ij}(x,\mathbf{y},t)\,n_j dY - \int_{\mathcal{Y}} \hat{z}_{,y_j}\sigma^2_{ij}(x,\mathbf{y},t)\,dV\end{aligned} \tag{2.57}$$

Proceeding further as in previous case, the equilibrium equation for moment resultant is received as follows.

$$\mathcal{M}_{\alpha\beta,x_\beta}(x,t) - \mathcal{Q}_\alpha(x,t) + p_\alpha(x,t) = \langle\rho\hat{z}\rangle\,\ddot{u}_\alpha(x,t) - \left\langle\rho\hat{z}^2\right\rangle\ddot{w}_{,x_\alpha}(x,t) \tag{2.58}$$

where,

$$p_\alpha(x,t) = \langle\hat{z}b_\alpha\rangle(x,t) + \left\langle\left(c^+ - \langle z\rangle\right)G_+\right\rangle_Y\bar{\tau}^+_\alpha(x,t) + \left\langle\left(c^- - \langle z\rangle\right)G_-\right\rangle_Y\bar{\tau}^-_\alpha(x,t) \tag{2.59}$$

Averaging the $O(\zeta^2)$ momentum balance equation (Eq. 2.27d) over the RVE, and using $O(\zeta^3)$ boundary condition yields:

$$\mathcal{Q}_{\alpha,x_\alpha}(x,t) + m(x,t) = \langle\rho\rangle\,\ddot{w}(x,t) \tag{2.60}$$

in which,

$$m\left(x,t\right)=\left\langle b_3\right\rangle\left(x,t\right)+\left\langle G_+\right\rangle_Y\bar{\tau}_3^+\left(x,t\right)+\left\langle G_-\right\rangle_Y\bar{\tau}_3^-\left(x,t\right) \tag{2.61}$$

Following the definition of $N_{\alpha\beta}$, after some rearrangement, the constitutive equation for $\mathcal{N}_{\alpha\beta}$ can be written in the following form.

$$\begin{aligned}\mathcal{N}_{\alpha\beta}\left(x,t\right)=&A^{\mathcal{Y}}_{\alpha\beta\mu\eta}e_{\mu\eta}\left(x,t\right)+E^{\mathcal{Y}}_{\alpha\beta\mu\eta}\kappa_{\mu\eta}\left(x,t\right)+\\&\int_{\mathcal{Y}}T^{\mathcal{Y}}_{\alpha\beta kl}\left(\hat{\mathbf{y}}\right)\bar{\mu}_{kl}\left(x,\hat{\mathbf{y}},t\right)d\hat{\mathbf{y}}+\int_{\mathcal{Y}}H^{\mathcal{Y}}_{\alpha\beta kl}\left(\hat{\mathbf{y}}\right)\hat{\mu}_{kl}\left(x,\hat{\mathbf{y}},t\right)d\hat{\mathbf{y}}\end{aligned} \tag{2.62}$$

where,

$$A^{\mathcal{Y}}_{ij\alpha\beta} = \left\langle L_{ijkl}\left(\mathbf{y}\right)A_{kl\alpha\beta}\left(\mathbf{y}\right)\right\rangle \tag{2.63}$$

$$E^{\mathcal{Y}}_{ij\alpha\beta} = \left\langle L_{ijkl}\left(\mathbf{y}\right)E_{kl\alpha\beta}\left(\mathbf{y}\right)\right\rangle \tag{2.64}$$

$$T^{\mathcal{Y}}_{\alpha\beta kl} = \left\langle L_{\alpha\beta mn}\left(\mathbf{y}\right)\tilde{A}_{mnkl}\left(\mathbf{y},\hat{\mathbf{y}}\right)\right\rangle \tag{2.65}$$

$$H^{\mathcal{Y}}_{\alpha\beta kl} = \left\langle L_{\alpha\beta mn}\left(\mathbf{y}\right)\tilde{E}_{mnkl}\left(\mathbf{y},\hat{\mathbf{y}}\right)\right\rangle \tag{2.66}$$

Similarly, moment resultant $\mathcal{M}_{\alpha\beta}(x,t)$ can abe written as following.

$$\begin{aligned}\mathcal{M}_{\alpha\beta}\left(x,t\right)=F^{\mathcal{Y}}_{\alpha\beta\mu\eta}e_{\mu\eta}\left(x,t\right)+D^{\mathcal{Y}}_{\alpha\beta\mu\eta}\kappa_{\mu\eta}\left(x,t\right)\\+\int_{\mathcal{Y}}G^{\mathcal{Y}}_{\alpha\beta kl}\left(\hat{\mathbf{y}}\right)\bar{\mu}_{kl}\left(x,\hat{\mathbf{y}},t\right)d\hat{\mathbf{y}}+\int_{\mathcal{Y}}C^{\mathcal{Y}}_{\alpha\beta kl}\left(\hat{\mathbf{y}}\right)\hat{\mu}_{kl}\left(x,\hat{\mathbf{y}},t\right)d\hat{\mathbf{y}}\end{aligned} \tag{2.67}$$

where,

$$F^{\mathcal{Y}}_{\alpha\beta\mu\eta} = \langle \hat{z} L_{\alpha\beta\gamma\xi}(\mathbf{y}) A_{\gamma\xi\mu\eta}(\mathbf{y}) \rangle \tag{2.68}$$

$$D^{\mathcal{Y}}_{\alpha\beta\mu\eta} = \langle \hat{z} L_{\alpha\beta\gamma\xi}(\mathbf{y}) E_{\gamma\xi\mu\eta}(\mathbf{y}) \rangle \tag{2.69}$$

$$G^{\mathcal{Y}}_{\alpha\beta kl}(\hat{\mathbf{y}}) = \left\langle \hat{z} L_{\alpha\beta ij}(\mathbf{y}) \tilde{A}_{ijkl}(\mathbf{y}, \hat{\mathbf{y}}) \right\rangle \tag{2.70}$$

$$C^{\mathcal{Y}}_{\alpha\beta kl}(\hat{\mathbf{y}}) = \left\langle \hat{z} L_{\alpha\beta ij}(\mathbf{y}) \tilde{E}_{ijkl}(\mathbf{y}, \hat{\mathbf{y}}) \right\rangle \tag{2.71}$$

2.8 Boundary Conditions

To complete the formulation of the macroscopic problem, it remains to define the boundary conditions along Γ_0, which are assumed to be of the following form:

$$u^{\zeta}_i(\mathbf{x}, t) = r^{\zeta}(\mathbf{x}, t); \quad \text{on } \Gamma^r_0 \tag{2.72}$$

$$\sigma^{\zeta}_{ij}(\mathbf{x}, t) n_j = \tau^{\zeta}_i(\mathbf{x}, t); \quad \text{on } \Gamma^{\tau}_0 \tag{2.73}$$

where, boundary partitions satisfy: $\Gamma_0 = \Gamma^r_0 \cup \Gamma^{\tau}_0$, $\Gamma^r_0 \cap \Gamma^{\tau}_0 = \emptyset$. Along the displacement boundaries, Γ^r_0, the displacement data of the following form is admitted

$$r^{\zeta}(\mathbf{x}, t) = \delta_{i3} W(x, t) + \zeta \delta_{i\alpha} [r_{\alpha}(x, t) - \hat{z}\theta_{\alpha}(x, t)] \tag{2.74}$$

Matching the displacement terms of zeroth and first orders along the boundary gives

$$O(1): \quad w(x, t) = W(x, t) \tag{2.75}$$

$$O(\zeta): \quad u_{\alpha} - \hat{z} w_{,x_{\alpha}} = r_{\alpha}(x, t) - \hat{z}\theta_{\alpha}(x, t) \tag{2.76}$$

Averaging Eq. 2.76 over the RVE boundary gives the remaining displacement and rotation boundary conditions

$$u_\alpha = r_\alpha; \quad w_{,x_\alpha} = \theta_\alpha; \quad \text{on } \Gamma_0^r \tag{2.77}$$

Along the traction boundaries, Γ_0^τ, the traction data is assumed to satisfy the following scaling relations with respect to ζ

$$\tau_i^\zeta = \zeta \delta_{i\alpha} \tau_\alpha (x,t) + \zeta^2 \delta_{i3} \tau_3 (x,t) \tag{2.78}$$

The traction boundaries are satisfied approximately in the integral form. The equivalence relation between the average and exact boundary conditions may be shown based on the Saint Venant principle [2]. The moment, force and shear resultant boundary conditions are given as:

$$\mathcal{N}_{\alpha\beta} n_\beta = \tau_\alpha; \quad \mathcal{M}_{\alpha\beta} n_\beta = \langle \hat{z} \rangle \tau_\alpha; \quad \mathcal{Q}_\alpha n_\alpha = \tau_3 \tag{2.79}$$

Boundary data is taken to satisfy the free-edge condition [3].

CHAPTER III

FORMULATION OF REDUCED ORDER THIN PLATE PROBLEM

3.1 Reduced Order Model of Damage Variable and Inelastic Strains

In order to reduce the computational cost of direct homogenization, the constitutive relations developed in Sec. 2.7 are homogenized over reduced order model. This type of decomposition of the RVE is also consistent with TFA implementation for eigenstrains (See Sec. 1.5). This is introduced using separation of variables for damage induced total inelastic strain and damage variable as following [29].

$$\omega_{ph}(\mathbf{x},\mathbf{y},t) = \sum_{\gamma} N_{ph}^{(\gamma)}(\mathbf{y})\omega_{ph}^{(\gamma)}(\mathbf{x},t) \tag{3.1}$$

$$\mu_{ij}(\mathbf{x},\mathbf{y},t) = \sum_{\gamma} N_{ph}^{(\gamma)}(\mathbf{y})\mu_{ij}^{(\gamma)}(\mathbf{x},t) \tag{3.2}$$

The phase shape function, $N_{ph}^{(\gamma)}(\mathbf{y})$ are assumed to be C^{-1} continuous in RVE in order to match the continuity of the displacement derivatives. In addition, the assumed shape function $N_{ph}^{(\gamma)}(\mathbf{y})$ needs to satisfy the partition of unity property, i.e.

$$\sum_{\gamma} N_{ph}^{(\gamma)}(\mathbf{y}) = 1 \tag{3.3}$$

The weighted average of the various fields are defined as follows.

$$\omega_{ph}^{(\gamma)}(\mathbf{x},t) = \int_V \psi_{ph}^{(\gamma)}(\mathbf{y})\omega_{ph}(\mathbf{x},\mathbf{y},t)\,dy \tag{3.4}$$

$$\mu_{ph}^{(\gamma)}(\mathbf{x},t) = \int_V \psi_{ph}^{(\gamma)}(\mathbf{y})\mu_{ph}(\mathbf{x},\mathbf{y},t)\,dy \tag{3.5}$$

where, the phase weight function $\psi_{ph}^{(\gamma)}$ satisfy positivity and normality conditions, as shown below.

$$\psi_{ph}^{(\gamma)}(\mathbf{y}) \geq 0 \tag{3.6}$$

$$\int_V \psi_{ph}^{(\gamma)}(\mathbf{y})dy = 1 \tag{3.7}$$

Therefore, for arbitrary state of damage, the phase shape function and weight functions are orthonormal to each other, i.e.

$$\int_V \psi_{ph}^{(\gamma)}(\mathbf{y}) N_{ph}^{(\eta)}(\mathbf{y})dy = \delta_{\gamma\eta} \tag{3.8}$$

where, $\delta_{\gamma\eta}$ is the Kronecker delta.

Consider a two scale heterogeneous material composed of n_{ph} constituent phases. The RVE microstructure is further subdivided into n subdomains denoted by V^{η}, $\eta = 1, 2, 3, ..., n$. The RVE is partitioned in such a way that each subdomain belongs to a single phase, i.e. if M denotes the matrix and F denotes the fiber, then $V_{(\eta)} \bigcap V_{(M)} \equiv V^{(\eta)}$ or $V_{(\eta)} \bigcap V_{(F)} \equiv V^{(\eta)}$, $V \equiv \bigcup_{\eta=1}^{n} V^{(\eta)}$ and $V^{(\eta)} \bigcup V^{(\upsilon)} \equiv 0$ for $\eta \neq \upsilon$. The assumed shape and weight functions ($N_{ph}^{(\gamma)}$ and $\psi_{ph}^{(\gamma)}$, respectively) are selected to be piecewise constant in V with nonzero values within their corresponding partitions, $V^{(\gamma)}$, only

$$N_{ph}^{(\gamma)}(\mathbf{y}) = \begin{cases} 1, \text{if y} \in V^{(\eta)} \\ 0, elsewhere \end{cases} \tag{3.9}$$

$$\psi_{ph}^{(\gamma)}(\mathbf{y}) = \frac{1}{V^{(\eta)}} N_{ph}^{(\gamma)}(\mathbf{y}) \tag{3.10}$$

where, $|V^{(\eta)}|$ is the volume of partition $V^{(\eta)}$. This definition of the subdomains divided RVE volume V into noncontiguous subdomains.

The phase averages of damage variable and eigenstrains, due to in-plane deformation $\bar{\mu}_{ij}$ and bending deformation $\hat{\mu}_{ij}$, for reduced order homogenization are introduced as follows.

$$\left\{ \begin{array}{c} \bar{\mu}_{ij} \\ \hat{\mu}_{ij} \\ \omega \end{array} \right\} (x, \mathbf{y}, t) = \sum_{I=1}^{n} \left\{ \begin{array}{c} \bar{N}^{(I)}(\mathbf{y}) \bar{\mu}_{ij}^{(I)}(x,t) \\ \hat{N}^{(I)}(\mathbf{y}) \hat{\mu}_{ij}^{(I)}(x,t) \\ \vartheta^{(I)}(\mathbf{y}) \omega^{(I)}(x,t) \end{array} \right\} \tag{3.11}$$

where, $\bar{N}^{(I)}$, $\hat{N}^{(I)}$ and $\vartheta^{(I)}$ are shape functions, and; $\bar{\mu}_{ij}^{(I)}$, $\hat{\mu}_{ij}^{(I)}$ and $\omega^{(I)}(x,t)$ are the weight averaged planar deformation, bending induced inelastic strain and damage fields, respectively:

$$\left\{ \begin{array}{c} \bar{\mu}_{ij}^{(I)} \\ \hat{\mu}_{ij}^{(I)} \\ \omega^{(I)} \end{array} \right\} (x,t) = \int_{\mathcal{Y}} \left\{ \begin{array}{c} \bar{\psi}^{(I)}(\mathbf{y}) \bar{\mu}_{ij}(x, \mathbf{y}, t) \\ \hat{\psi}^{(I)}(\mathbf{y}) \hat{\mu}_{ij}(x, \mathbf{y}, t) \\ \eta^{(I)}(\mathbf{y}) \omega(x, \mathbf{y}, t) \end{array} \right\} d\mathbf{y} \tag{3.12}$$

where, $\bar{\psi}^{(I)}$, $\hat{\psi}^{(I)}$ and $\eta^{(I)}$ are microscopically nonlocal weight functions. The shape functions are taken to satisfy partition of unity property, while the weight are positive, normalized and orthonormal with respect to shape functions as described previously. This discretization of macroscopic and microscopic inelastic strains results in reduction in number of kinematic equations for the system which in turn further improves the computation efficiency of the model. However, this discretization is not a required condition for solution.

Now, consider in-elastic strain developed due to in-plane deformation.

$$\bar{\mu}_{ij}\left(x,\mathbf{y},t\right)=\omega\left(x,\mathbf{y},t\right)\epsilon_{ij}^{1}\left(x,\mathbf{y},t\right) \tag{3.13}$$

Expanding this with the help of Eqs. 2.22a and 2.6, one gets

$$\begin{aligned}\bar{\mu}_{ij}\left(x,\mathbf{y},t\right)=\omega\left(x,\mathbf{y},t\right)\left[\delta_{i\alpha}\delta_{j\beta}e_{\alpha\beta}\left(x,t\right)+\frac{1}{2}\{\delta_{i3}\delta_{j\alpha}+\delta_{i\alpha}\delta_{j3}\}u_{3,x_{\alpha}}\left(x,t\right)\right.\\ \left.+\Theta_{(i,y_j)\alpha\beta}(\mathbf{y},t)e_{\alpha\beta}(x,t)+\int_{\mathcal{Y}}\tilde{\Theta}_{(i,y_j)kl}(y,\hat{y})\bar{\mu}\left(x,\hat{\mathbf{y}},t\right)d\hat{y}\right]-\left(\hat{z}\delta_{i\alpha}u_{3,x_{\alpha}}\left(x,t\right)\right)_{,y_j}\end{aligned} \tag{3.14}$$

Consider the fact that u_3 is independent of microscopic scale and define the following:

Define:

$$\mathcal{A}_{ij\alpha\beta}=I_{ij\alpha\beta}+\Theta_{(i,y_j)\alpha\beta}(\mathbf{y},t)$$

Plugging the $\mathcal{A}_{ij\alpha\beta}$ and $\bar{\mu}\left(x,\hat{\mathbf{y}},t\right)$ from Eq. 3.11 in the last expression yields the following.

$$\begin{aligned}\bar{\mu}_{ij}\left(x,\mathbf{y},t\right)=\omega\left(x,\mathbf{y},t\right)\left[\mathcal{A}_{ij\alpha\beta}e_{\alpha\beta}(x,t)\right.\\ \left.+\sum_{J}\int_{\mathcal{Y}}\tilde{\Theta}_{(i,y_j)kl}(y,\hat{y})\bar{N}^{(J)}(\hat{\mathbf{y}})\bar{\mu}^{(J)}\left(x,t\right)d\hat{y}\right]\end{aligned} \tag{3.15}$$

or,

$$\begin{aligned}\bar{\mu}_{ij}\left(x,\mathbf{y},t\right)=&\omega\left(x,\mathbf{y},t\right)\left[\mathcal{A}_{ij\alpha\beta}e_{\alpha\beta}(x,t)\right.\\ &\left.+\sum_{J}P_{ijkl}^{(J)}(\mathbf{y})\bar{\mu}^{(J)}\left(x,t\right)\right]\end{aligned} \tag{3.16}$$

where,

$$P_{ijkl}(\mathbf{y}) = \int_{\mathcal{Y}} \tilde{\Theta}_{(i,y_j)kl}(y,\hat{y})\bar{N}^{(J)}(\hat{\mathbf{y}})d\hat{y}$$

Now, the both sides of the last equation are multiplied by $\bar{\psi}^{(I)}(\mathbf{y})$ and the reduced order expression for damage variable is plugged in the last equation, then the resulting equation is integrated over the unit cell, which yields the following expressions.

$$\begin{aligned}\int_{\mathcal{Y}} \bar{\mu}_{ij}\left(x,\mathbf{y},t\right)\bar{\psi}^{(I)}(\mathbf{y})d\mathbf{y} = \int_{\mathcal{Y}} \omega\left(x,t\right)\vartheta^{(I)}(\mathbf{y})\bar{\psi}^{(I)}(\mathbf{y})\mathcal{A}_{ij\alpha\beta}e_{\alpha\beta}(x,t)d\mathbf{y} \\ + \sum_J \int_{\mathcal{Y}} \omega\left(x,t\right)\vartheta^{(I)}(\mathbf{y})\bar{\psi}^{(I)}(\mathbf{y})P^{(J)}_{ijkl}(\mathbf{y})\bar{\mu}^{(J)}\left(x,t\right)d\mathbf{y}\end{aligned} \tag{3.17}$$

or,

$$\bar{\mu}^{(I)}_{ij}(x,t) = \omega^{(I)}(x,t)\left(A^{(I)}_{ij\mu\eta}e_{\mu\eta}(x,t) + \sum_J P^{(IJ)}_{ijkl}\bar{\mu}^{(J)}_{kl}(x,t)\right) \tag{3.18}$$

Similar treatment for in-elastic strains due to bending yields the following expression for $\hat{\mu}^{(I)}_{ij}(x,t)$.

$$\hat{\mu}^{(I)}_{ij}(x,t) = \omega^{(I)}(x,t)\left(E^{(I)}_{ij\mu\eta}\kappa_{\mu\eta}(x,t) + \sum_J Q^{(IJ)}_{ijkl}\hat{\mu}^{(J)}_{kl}(x,t)\right) \tag{3.19}$$

where,

$$P^{(I)}_{ijkl}\left(\mathbf{y}\right) = \int_{\mathcal{Y}} \bar{N}^{(I)}\left(\mathbf{y}\right)\tilde{\Theta}_{(i,y_j)kl}\left(\mathbf{y}\right)d\mathbf{y} \tag{3.20}$$

$$Q^{(I)}_{ijkl}(\mathbf{y}) = \int_{\mathcal{Y}} \hat{N}^{(I)}(\mathbf{y})\,\tilde{\Xi}_{(i,y_j)kl}(\mathbf{y})\,d\mathbf{y} \tag{3.21}$$

$$A^{(I)}_{ij\mu\eta} = \int_{\mathcal{Y}} \bar{\psi}^{(I)}(\mathbf{y})\vartheta^{(I)}(\mathbf{y})A_{ij\mu\eta}(\mathbf{y})\,d\mathbf{y} \tag{3.22}$$

$$E^{(I)}_{ij\mu\eta} = \int_{\mathcal{Y}} \hat{\psi}^{(I)}(\mathbf{y})\vartheta^{(I)}(\mathbf{y})E_{ij\mu\eta}(\mathbf{y})\,d\mathbf{y} Q^{(IJ)}_{\alpha\beta\mu\eta} = \int_{\mathcal{Y}} \hat{\psi}^{(I)}(\mathbf{y})\vartheta^{(I)}(\mathbf{y})Q^{(J)}_{\alpha\beta\mu\eta}(\mathbf{y})\,d\mathbf{y} \tag{3.23}$$

The damage induced inelastic strain tensors $\bar{\mu}_{ij}$ and $\hat{\mu}_{ij}$ account for the coupling between the microscopic and macroscopic problems, where $\bar{\mu}_{ij}$ describes inelastic strain due to in-plane deformation and $\hat{\mu}_{ij}$ is inelastic strain due to bending.

3.2 Reduced Order Model of Constitutive Equations

Next step involves the development of reduced order form of thin plate constitutive Eqs. 2.7 and 2.67. First consider Eq. 2.7.

$$\begin{aligned}\mathcal{N}_{\alpha\beta}(x,t) =& A^{\mathcal{Y}}_{\alpha\beta\mu\eta}e_{\mu\eta}(x,t) + E^{\mathcal{Y}}_{\alpha\beta\mu\eta}\kappa_{\mu\eta}(x,t) + \\ & \int_{\mathcal{Y}} T^{\mathcal{Y}}_{\alpha\beta kl}(\hat{\mathbf{y}})\,\bar{\mu}_{kl}(x,\hat{\mathbf{y}},t)\,d\hat{\mathbf{y}} + \int_{\mathcal{Y}} H^{\mathcal{Y}}_{\alpha\beta kl}(\hat{\mathbf{y}})\,\hat{\mu}_{kl}(x,\hat{\mathbf{y}},t)\,d\hat{\mathbf{y}}\end{aligned}$$

where, expressions for $T^{\mathcal{Y}}_{ijkl}$ and $H^{\mathcal{Y}}_{ijkl}$ are given in Eq. 2.63.

Consider the third term of the right side of the above equation and plug in the expressions for $T^{\mathcal{Y}}_{ijkl}$ from Eq. 2.63, where $\tilde{A_{ijkl}}$ is given by Eq. 2.43.

$$\int_{\mathcal{Y}} T^{\mathcal{Y}}_{\alpha\beta kl}(\hat{\mathbf{y}})\,\bar{\mu}(x,\hat{\mathbf{y}},t)d\hat{y} = \int_{\mathcal{Y}} \left\langle L_{ijmn}(\mathbf{y})\left\{\tilde{\Theta}_{(i,y_j)kl}(\mathbf{y},\hat{\mathbf{y}}) - d(\hat{\mathbf{y}}-\mathbf{y})\,I_{ijkl}\right\}\right\rangle \bar{\mu}_{kl}(x,\hat{\mathbf{y}},t)d\hat{\mathbf{y}} \tag{3.24}$$

Substituting the reduced order expression for $\bar{\mu}(x,\hat{\mathbf{y}},t)$ in the above equation yields the following.

$$\int_{\mathcal{Y}} T^{\mathcal{Y}}_{\alpha\beta kl}\left(\hat{\mathbf{y}}\right)\bar{\mu}(x,\hat{\mathbf{y}},t)d\hat{y} = \sum_{I}\int_{\mathcal{Y}}\{\Big\langle L_{ijmn}\left(\mathbf{y}\right)\{\tilde{\Theta}_{(i,y_j)kl}\left(\mathbf{y},\hat{\mathbf{y}}\right) - d\left(\hat{\mathbf{y}}-\mathbf{y}\right)I_{ijkl}\}\Big\rangle$$
$$N^{(I)}(\hat{\mathbf{y}})\bar{\mu}^{(I)}_{kl}(x,t)\}d\hat{\mathbf{y}} \tag{3.25}$$

or,

$$\int_{\mathcal{Y}} T^{\mathcal{Y}}_{\alpha\beta kl}\left(\hat{\mathbf{y}}\right)\bar{\mu}(x,\hat{\mathbf{y}},t)d\hat{y} = \sum_{I} T^{(I)}_{\alpha\beta kl}\bar{\mu}^{(I)}_{kl}(x,t) \tag{3.26}$$

where,

$$T^{(I)}_{\alpha\beta kl} = \Big\langle L_{\alpha\beta ij}(\mathbf{y})\left[P^{(I)}_{ijkl}(\mathbf{y}) - I_{ijkl}\bar{N}^{(I)}(\mathbf{y})\right]\Big\rangle \tag{3.27}$$

where, $P^{(I)}_{ijkl}(\mathbf{y})$ is given by Eq. 3.20.

Similar treatment is given to the fourth right hand side term of the Eq. 2.7, which yields in-plane force resultant in terms of phase average fields as shown below.

$$\mathcal{N}_{\alpha\beta}\left(x,t\right) = A^{\mathcal{Y}}_{\alpha\beta\mu\eta}e_{\mu\eta}\left(x,t\right) + E^{\mathcal{Y}}_{\alpha\beta\mu\eta}\kappa_{\mu\eta}\left(x,t\right) + \sum_{I=1}^{n}\left(T^{(I)}_{\alpha\beta kl}\bar{\mu}^{(I)}_{kl}\left(x,t\right) + H^{(I)}_{\alpha\beta kl}\hat{\mu}^{(I)}_{kl}\left(x,t\right)\right) \tag{3.28}$$

where,

$$H^{(I)}_{\alpha\beta kl} = \Big\langle L_{\alpha\beta ij}(\mathbf{y})\left[Q^{(I)}_{ijkl}(\mathbf{y}) - I_{ijkl}\hat{N}^{(I)}(\mathbf{y})\right]\Big\rangle \tag{3.29}$$

where, $Q^{(I)}_{ijkl}(\mathbf{y})$ is given by Eq. 3.21.

The reduced order expression for the moment resultant constitutive equation (Eq 2.67) is also derived following similar steps as described above for Eq. 3.28. The

expression for moment resultant in terms of phase average fields is given as follows.

$$\mathcal{M}_{\alpha\beta}(x,t) = F^{\mathcal{Y}}_{\alpha\beta\mu\eta} e_{\mu\eta}(x,t) + D^{\mathcal{Y}}_{\alpha\beta\mu\eta}\kappa_{\mu\eta}(x,t) + \sum_{I=1}^{n}\left(G^{(I)}_{\alpha\beta kl}\bar{\mu}^{(I)}_{kl}(x,t) + C^{(I)}_{\alpha\beta kl}\hat{\mu}^{(I)}_{kl}(x,t)\right) \tag{3.30}$$

where,

$$G^{(I)}_{\alpha\beta kl} = \left\langle \hat{z} L_{\alpha\beta ij}(\mathbf{y}) \left[P^{(I)}_{ijkl}(\mathbf{y}) - I_{ijkl}\bar{N}^{(I)}(\mathbf{y}) \right] \right\rangle \tag{3.31}$$

$$C^{(I)}_{\alpha\beta kl} = \left\langle \hat{z} L_{\alpha\beta ij}(\mathbf{y}) \left[Q^{(I)}_{ijkl}(\mathbf{y}) - I_{ijkl}\hat{N}^{(I)}(\mathbf{y}) \right] \right\rangle \tag{3.32}$$

3.3 Rate dependent damage evolution model

The inelastic processes within the microstructure is idealized using the damage variables, $\omega^{(I)}$. In this manuscript a rate-dependent model is used to characterize the evolution of damage within the microstructure. A Perzyna-type viscoplastic regularization of classical rate independent models [32] is employed to alleviate the mesh size senstivity problem.

A potential damage function, f, is defined:

$$f\left(\upsilon^{(I)}, r^{(I)}\right) = \phi\left(\upsilon^{(I)}\right) - \phi\left(r^{(I)}\right) \leqslant 0 \tag{3.33}$$

in which, $\upsilon^{(I)}(x,t)$ and $r^{(I)}(x,t)$ are phase damage equivalent strain and damage hardening variable, respectively, and; ϕ is a monotonically increasing damage evolution function. The evolution equations for $\upsilon^{(I)}$ and $r^{(I)}$ are given as

$$\dot{\omega}^{(I)} = \dot{\lambda}\frac{\partial\phi}{\partial\upsilon^{(I)}} \tag{3.34}$$

$$\dot{r}^{(I)} = \dot{\lambda} \tag{3.35}$$

where the evolution is based on a power law expression of the form:

$$\dot{\lambda} = \frac{1}{q^{(I)}} \left\langle f\left(\upsilon^{(I)}, r^{(I)}\right)\right\rangle_{+}^{p^{(I)}} \tag{3.36}$$

$\langle\cdot\rangle_{+} = [\|\cdot|+(\cdot)]/2$ denotes MacCauley brackets; $p^{(I)}$ and $q^{(I)}$ define the rate-dependent response of damage evolution.

The phase damage equivalent strain is defined as

$$\upsilon^{(I)} = \sqrt{\frac{1}{2}\left(\mathbf{F}^{(I)}\hat{\epsilon}^{(I)}\right)^{\mathrm{T}}\hat{\mathbf{L}}^{(I)}\left(\mathbf{F}^{(I)}\hat{\epsilon}^{(I)}\right)} \tag{3.37}$$

in which, $\hat{\pm\epsilon}^{(\eta)}$ is the average principal strain tensor in $\mathcal{Y}^{(I)}$; $\hat{\mathbf{L}}^{(I)}$ is the tensor of elastic moduli rotated onto the principal strain directions, and; $\mathbf{F}^{(I)}(\mathbf{x}, t)$ is the weighting matrix. The weighting matrix accounts for the anisotropic damage accumulation in tensile and compressive directions:

$$\mathbf{F}^{(\eta)} = \begin{bmatrix} h_1^{(I)} & 0 & 0 \\ 0 & h_2^{(I)} & 0 \\ 0 & 0 & h_3^{(I)} \end{bmatrix} \tag{3.38}$$

$$h_{\xi}^{(I)} = \frac{1}{2} + \frac{1}{\pi}\left(c_1^{(I)}\left(\hat{\epsilon}_{\xi}^{(I)} - c_2^{(I)}\right)\right) \tag{3.39}$$

where, material parameters, $c_1^{(I)}$ and $c_2^{(I)}$, control damage accumulation in tensile and compressive loading. A power law based damage evolution function is considered:

$$\phi^{(I)} = a^{(I)}\left\langle \upsilon^{(I)} - \upsilon_0^{(I)}\right\rangle_{\mathrm{M}}^{b^{(I)}}; \quad \phi^{(I)} \leq 1 \tag{3.40}$$

in which, $a^{(I)}$ and $b^{(I)}$ are material parameters. The analytical form of $\phi(r^(I))$ is obtained by replacing $v(I)$ by $r(I)$ in Eq. 3.33.

CHAPTER IV

RESULTS AND MODEL VERIFICATION

4.1 Numerical Implementation

The proposed multiscale model is implemented and incorporated into a commercial finite element analysis program (Abaqus). The implementation of proposed methodology in Abaqus is a two stage process as illustrated in Fig. 4.1. The first stage consists of the evaluation of first and second order RVE problems, summarized in chapter 2, and computation of coefficient tensors. The preprocessing stage is implemented via in-house code. The two linear elastic RVE problems are eveluated using the finite element method. The model order, n, is taken to be a user defined input variable which leads to a static partitioning strategy in which coefficient tensors remain constant throughout the macroscale analysis [35].

Classical rate independent damage models are well known to exhibit spurious mesh sensitivity in h-version when loading extends to the softening regime. This phenomenon is characterized by the localization of strains to within the size of a finite element. Multiscale failure models based on damage mechanics may show mesh sensitivity in all associated scales. The proposed multiscale model is microscopically nonlocal through the integral type nonlocal formulation presented in Sec. 3.2. In the macroscopic scales, mesh sensitivity is alleviated by considering the viscous regularization of the damage model [30], [31]. The commercial finite element software (Abaqus) is employed to evaluate the macroscopic boundary value problem. A user-defined generalized shell section behavior subroutine (UGENS) is implemented and

incorporated into Abaqus to update force and moments resultants. The UGENS subroutine consists of computation of force ($\mathcal{N}$) and moment ($\mathcal{M}$) resultant at current time step given the generalized macroscale strain tensors (e, κ) and the damage state variable, $\omega^{(I)}$ at the previous time step and the generalized strain increments. Numerical details of the update procedure to evaluate the constitutive response in UGENS is lengthy yet straight forward. A formulation of constitutive update based on reduced order damage models are provided in [29]. The Abaqus general purpose elements, S4R, are employed in thin plate simulations.

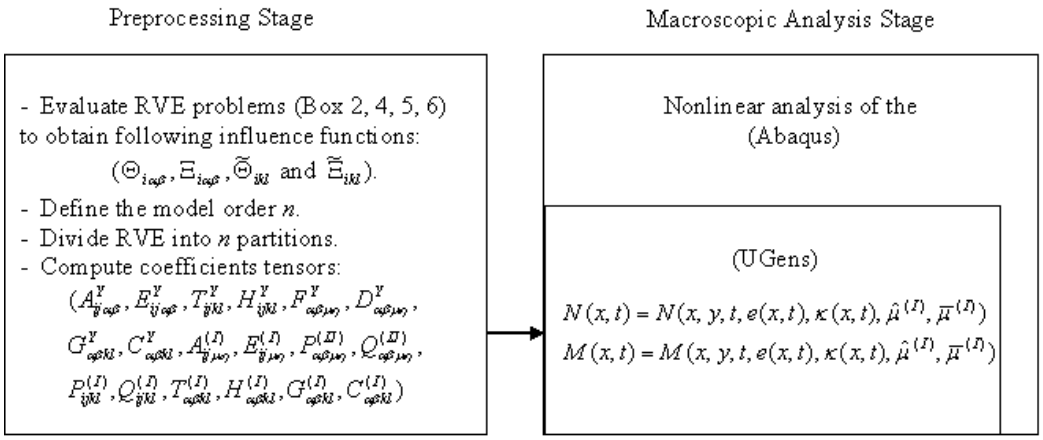

Figure 4.1. Flow Chart for Implementation of the Proposed Methodology in the Commercial Finite Element Code (Abaqus)

The capabilities of the proposed multiscale plate model is assessed by considering three test cases [35]: (a) 3-point bending; (b) uniaxial tension, and; (c) impact of rigid projectile on a woven composite plate. The model simulations are compared to direct 3-D (reference) finite element models in which the microstructure is resolved throughout the macro-structure.

4.2 Three Point Plate Bending Test

Consider a three-point bending of a simply supported composite plate as shown in Fig. 4.2. The dimensions of the rectangular plate are $W/L = 3/40$ and $t/L = 1/80$, in which t, W and L are the thickness, width and length of the plate, respectively. The small scaling parameter ζ can be calculated as the ratio between the thickness (or in-plane periodicity dimension) and the span length between the supports ($\epsilon = \zeta = 1/40$). A static vertical load is applied at the center of the plate quasi-statically until failure.

The microstructure consists of a matrix material reinforced with stiff unidirectional fibers oriented in the global z-direction as illustrated in Fig 4.2. The fiber fraction is 19% by volume. The stiffness contrast between the matrix and reinforcement phases is chosen to be $E^M/E^F = 0.3$, where, E^M and E^F are the Young's Moduli of matrix and fiber, respectively. Poisson's ratio of both the materials are assumed to be identical ($\nu^F = \nu^M$). Damage evolution parameters are chosen to assure a linear dependence between the damage equivalent strain and evolution law (i.e., in Eq. 3.40, $b^{(I)} = 1$). Damage is allowed to accumulate in tension only and no significant damage accumulation occurs under compressive loads. The fiber phase is assumed to be damage-free for the considered load amplitudes, and damage is allowed to accumulate in the matrix phase only.

A suite of multiscale model simulations are conducted to verify the proposed approach. three-, five-, thirteen- and twenty five- partition models are compared with 3-D reference simulations. The microstructural partitions for the 4 multiscale models are illustrated in Fig. 4.3. Simulations are conducted at 3-different load rates. An

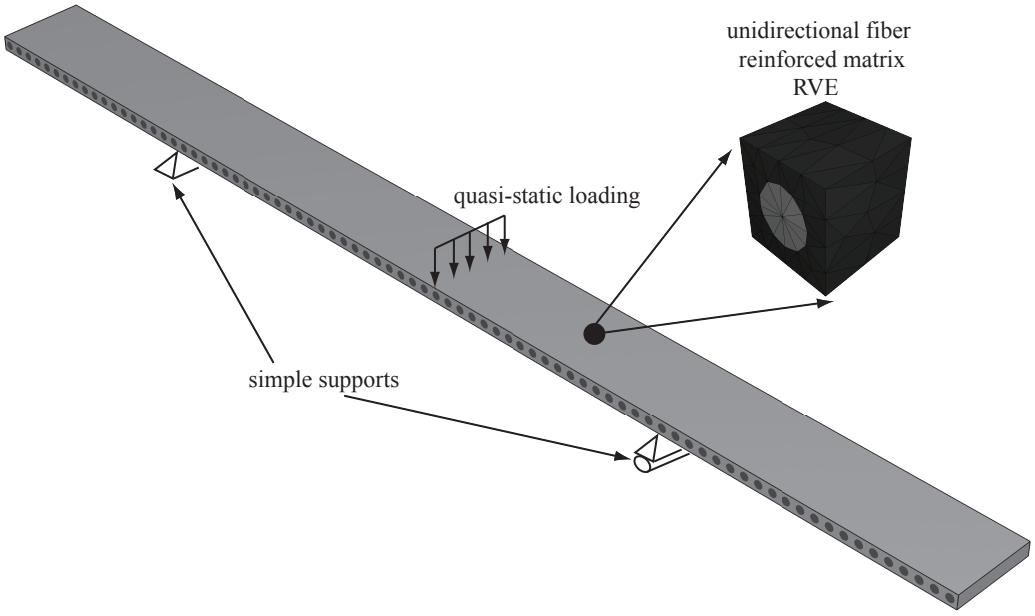

Figure 4.2. Macro- and microscopic configurations of the 3-point bending plate problem.

order of magnitude difference in the load rates are applied between the slow, intermediate and fast simulations. Fig. 4.4 illustrates the normalized force-displacement curves at the midspan of the plate. A reasonably good agreement is observed between the proposed multiscale models and reference simulations. The modeling error for the proposed models are tabulated in Table 1 for each multiscale model at each strain rate. It can be observed that while higher partition schemes tend to achieve better accuracy compared to lower partitions, a clear diminishing of error with increasing number of partitions does not occur. This is due to the non-optimal selection of the domains of each partition, which significantly affects the quality of the model.

Displacement profiles at failure illustrated in Fig. 4.5 also indicate similar trends observed above. The maximum error is observed in the 3-partition model simulations. Maximum normalized error occurs at the midspan of the plate (=6.5-9%). Damage contours at each partition of the 5-partition model is compared to

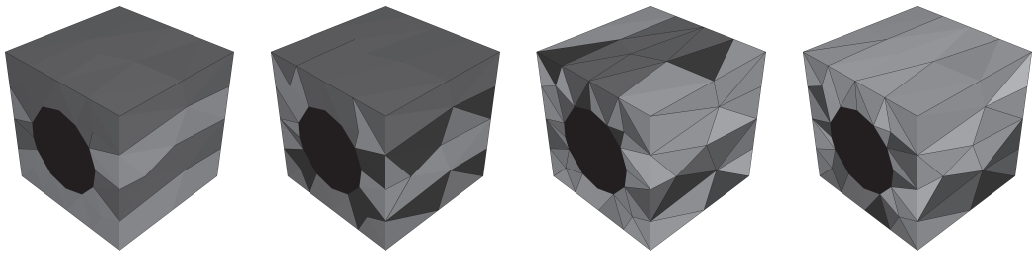

Figure 4.3. Microstructural partitioning for (a) 3-partition, (b) 5-partition, (c) 13-partition, and (d) 25-partition models. Each partition is identified using separate shades.

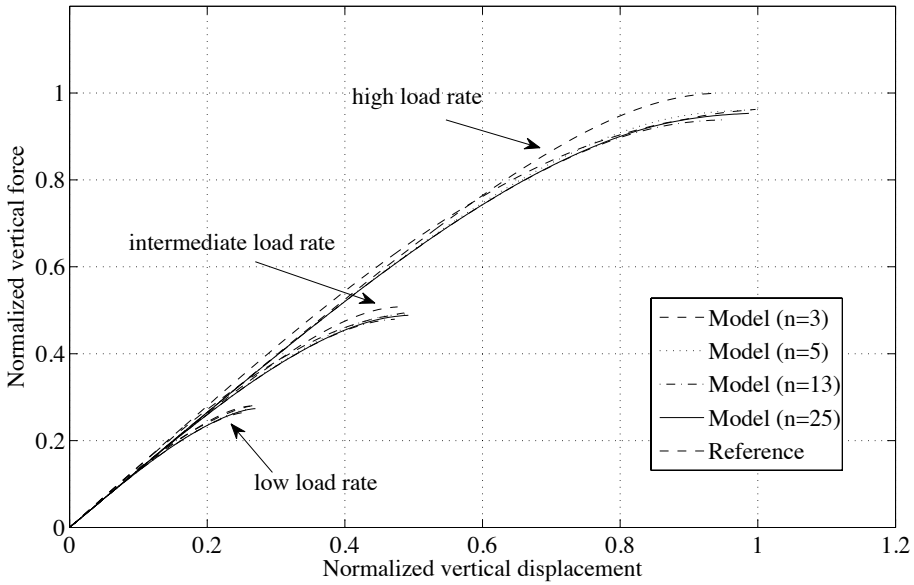

Figure 4.4. Normalized force-displacement curves in 3-point bending simulations. Multiscale simulation predictions compared to those of 3-D reference simulations.

Table 4.1. Errors in terms of failure displacement, failure force and L^2 norm in the force-displacement space.

2*Model	% error in failure displacement			% error in failure force			2% L^2 error		
	Slow	Int.	Fast	Slow	Int.	Fast	Slow	Int.	Fast
$n = 3$	2.8189	2.0079	5.4234	0.6942	2.8026	3.9114	0.0295	0.0878	0.1520
$n = 5$	2.1551	0.69527	0.32336	3.082	0.47734	0.0471	0.0642	0.0488	0.0457
$n = 13$	5.0153	2.8458	4.8786	5.7351	2.9361	2.4879	0.1095	0.0740	0.0622
$n = 25$	0.1385	1.2027	0.9786	2.7725	1.0971	0.9417	0.0921	0.0660	0.0540

the three-dimensional reference simulations in Fig. 4.6. The maximum damage is accumulated at the lowermost layer subjected to tensile loads. Upper layers are subjected to neutral and compressive loads leading to minimal damage accumulation. The 3-D reference analysis plots indicate that failure starts at the bottom of the plate, which is subjected to higher tensile stresses.

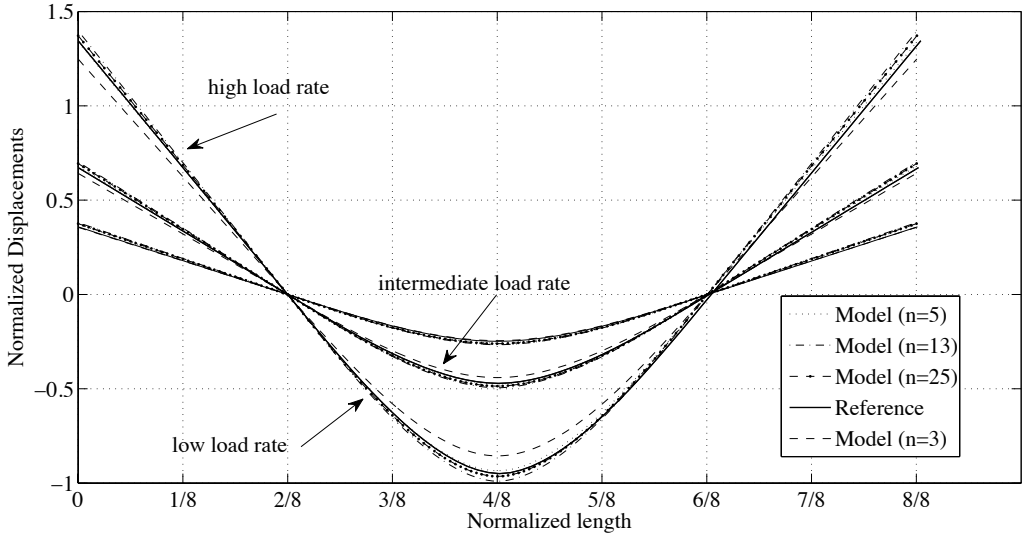

Figure 4.5. Comparison of displacements along the length of the plate, between the proposed multiscale models and 3-D reference problem.

4.3 Uniaxial Tension Test

The nonlocal characteristics of the proposed multiscale model using a uniaxially loaded thin rectangular plate are being reported hereinunder. The dimensions of the plate are $W/L = 1/5$ and $t/L = 1/30$. Two notches with half the thickness of the plate is placed at opposite edges of the plate, 45^0 apart. Prescribed displacements are applied along the in-plane dimension parallel to the long edge. The microstructural configuration and material properties are identical to the 3-point bending case discussed in the Sec. 4.2.

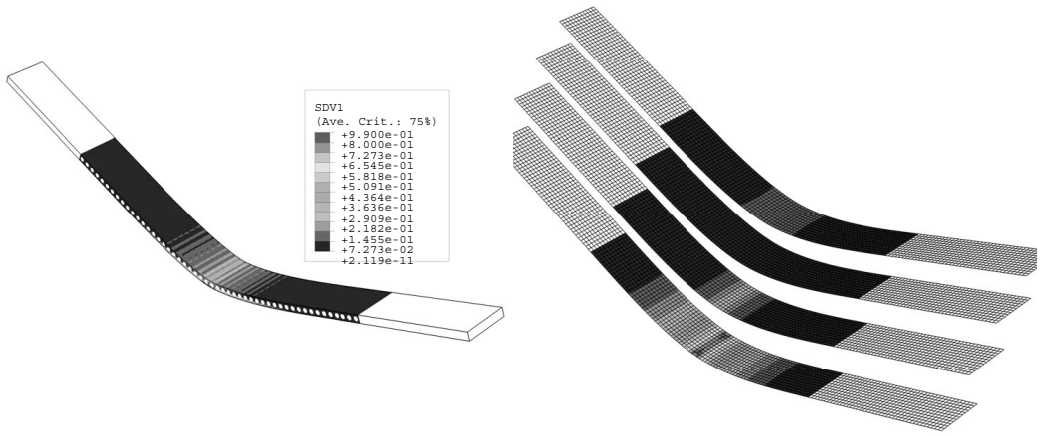

Figure 4.6. Damage profile for (a) 3-D reference simulation and, (b) 5-partition model. Damage variables plotted correspond to damage in each matrix partition in the 5-partition model.

A series of numerical simulations are conducted on three different finite element meshes with h/L ratios of 1/60, 1/120 and 1/240 as shown in Fig. 4.7. Two cases of microstructural orientation is considered: fibers are placed parallel and perpendicular to the stretch direction. Simulations are conducted using a 5-partition model ($n = 5$). Fig. 4.8 illustrates the damage fields ahead of the notches for the intermediate and fine meshes when the fibers are placed perpendicular to the loading direction. The contours correspond to the damage state at 75% of the failure displacement. The damage accumulation is observed to be along the direction of the elastic fibers. Fig. 4.9 illustrates the normalized force-displacement curves for coarse, intermediate and fine meshes. The softening regime of the curves for both microstructural orientations shows nearly identical response for all three meshes, clearly indicating the mesh independent characteristic of the proposed multiscale model. In the case of fibers parallel to the loading direction 166% and 140% increase have been observed in the failure

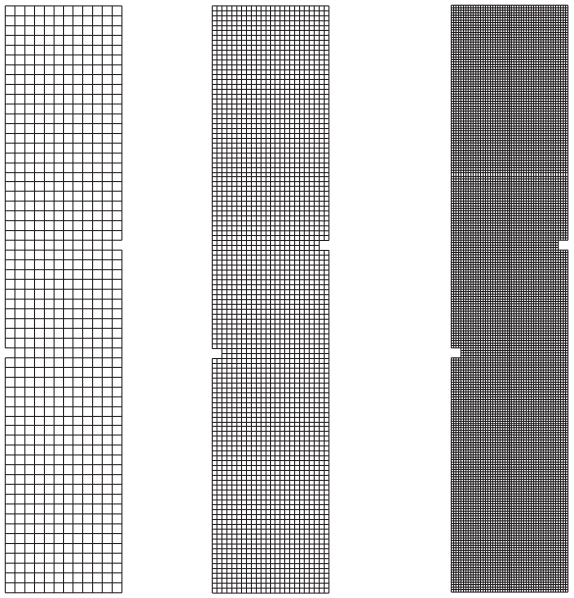

Figure 4.7. Finite element discretization of the macroscopic plates: (a) Coarse mesh ($h/L = 1/60$), (b) intermediate mesh ($h/L = 1/120$), and (c) fine mesh ($h/L = 1/240$).

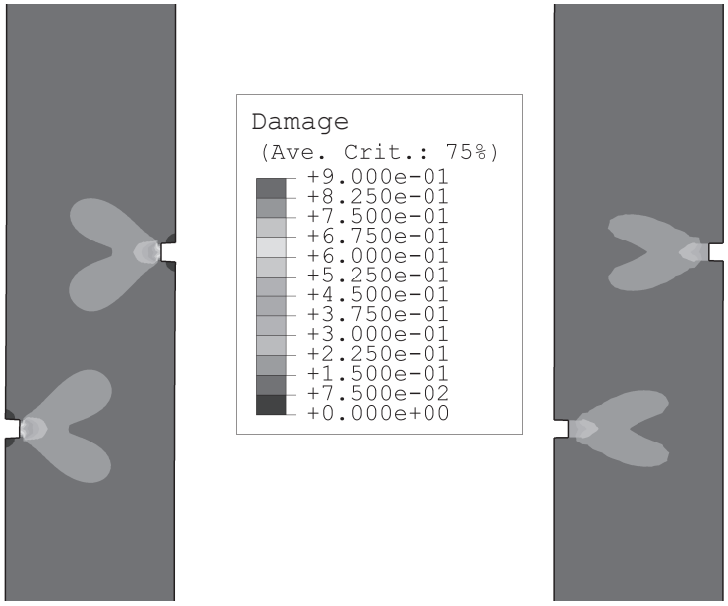

Figure 4.8. Damage contour plots for (a) fine mesh and, (b) intermediate mesh.

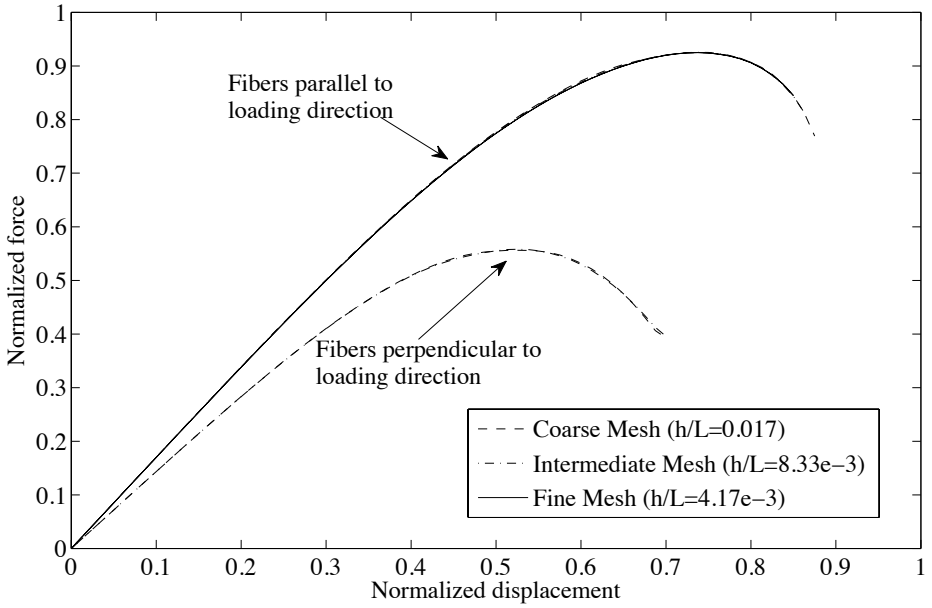

Figure 4.9. Force-displacement curves (normalized) simulated using coarse, intermediate and fine meshes for cases where fibers are placed parallel and perpendicular to the loading direction.

load and displacements, respectively.

4.4 High Velocity Impact Response of Woven Composite Plate

The capabilities of the proposed multiscale model is further verified by predicting the impact response of a composite plate. A 5-layer E-glass/polyester plain weave laminated composite system was experimentally investigated by Garcia-Castillo [36]. The microstructure of the composite laminated plate is illustrated in Fig. 4.10. The composite specimens are 140 mm by 200 mm rectangular plates with 3.19 mm thickness. The specimens were subjected to impact by steel projectiles with velocities ranging between 140-525 m/s. The proposed multiscale model is employed to predict the impact response of plates observed in the experiments. A 19-partition model is used here. The plate consists of 5- plain weave plies with 0.276 mm thickness. A

34.5 μm thick ply-interphase layer is assumed to exist between each ply. The weave tows are in 0- and 90- directions. The fiber volume fractions are 9% in 0-direction and 22% in the 90- direction with a total of 31%. The matrix, fiber tows in 0- and 90-directions and interphase in each layer is represented by a single partition totaling 19 for 5 plies.

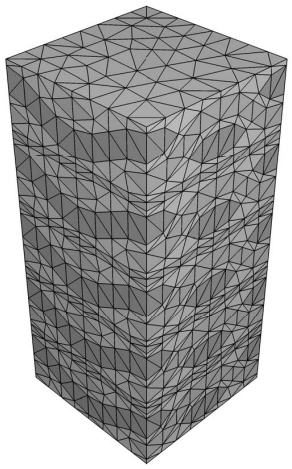

Figure 4.10. Microstructure of the 5-ply woven laminate system.

Failure in each partition is modeled using the rate-dependent damage model described in Sec. 3.3. Material properties of fiber tows in 0- and 90- directions are taken to be identical. The ply-interphase and matrix properties are also assumed to be identical. The static response of the composite system when subjected to uniaxial tension are used to calibrate $a^{(I)}$ and $b^{(I)}$ parameters for matrix and reinforcement by minimizing the discrepancy between the reported experimental failure stress and strain (3.6 % and 367 MPa). The SIMEX calibration model was used to conduct the calibration. SIMEX is a generic optimization framework for multiscale model calibration. The details of the SIMEX architecture are presented in [37]. The stress-strain curves based on uniaxial tension as well as damage evolution in each microconstituent

are shown in Fig. 4.11 for loading in two orthogonal directions. The damage evolution parameter $a^{(I)}$ and $b^{(I)}$ were determined as 0.08 and 1.5 for fiber, and 0.92 and 2.5 for matrix materials, respectively.

The fibers in 0- and 90-, as well as the matrix and interphase materials are assumed to have identical failure characteristics. A linear rate dependence is adopted for all microconstituents (i.e., $p^{(I)} = 1$). Damage is assumed to accumulate on the onset of loading ($\upsilon_0^{(I)} = 0$). Ply-interphase failure between all plies are observed in numerical simulations as indicated in Fig. 4.11, which is in agreement with the experimentally observed response [36]. In Fig. 11a and 11b illustrates the failure modes modeled in the simulations: Failure of the interphase between laminates, cracking within the matrix and and transverse directions. The effects of the fiber - matrix interface cracking is implicitly taken into account through the microconstituents cracking only. The failure of the interphase and the longitudinal fiber cracking (at 5% strain) precedes the matrix cracking (at 7% strain). The damage in the transverse fiber cracking remains low throughout the uniaxial loading. The exit velocities of the projectile when the composite specimen is subjected to impact velocities above the ballistic limit are predicted using the multiscale model. The experimentally provided ballistic limit value of 211 m/s is employed to calibrate the rate dependent material parameter of the microconstituent failure models ($q^{(I)} = 1.8e - 5$). Fig. 4.12 shows the exit velocity of the projectile as a function of the impact velocity. The simulated response shows a nonlinear relationship in impact velocities close to the ballistic limit followed by a linearizing trend - similar to the experimental observations. The discrepancy between the experimental observations and the simulated exit velocities are attributed to the limited data used in the calibration of the microconstituent material parameters.

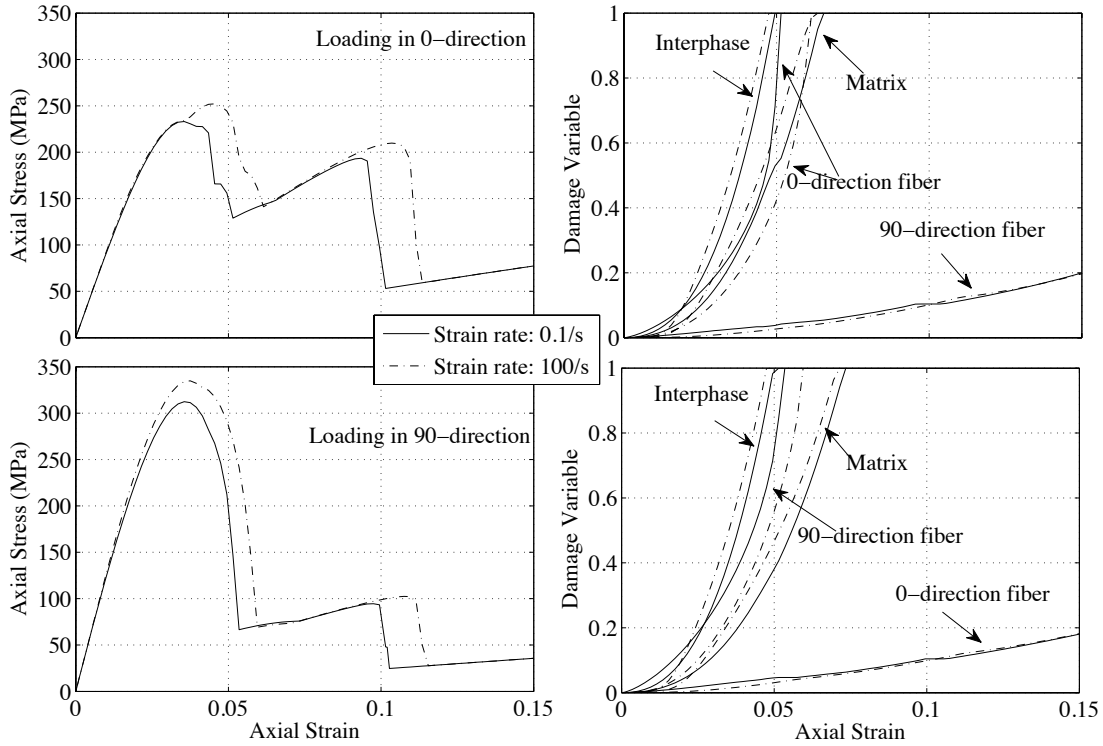

Figure 4.11. Simulations conducted under uniaxial tension: (a) Stress-strain curves when subjected to 0.1/s and 100/s strain rates in the 0-direction; (b) damage evolution in interphase, matrix and fiber phases for loading in the 0-direction; (c) stress-strain curves when subjected to 0.1/s and 100/s strain rates in the 90-direction; (d) damage evolution in interphase, matrix and fiber phases for loading in the 90-direction.

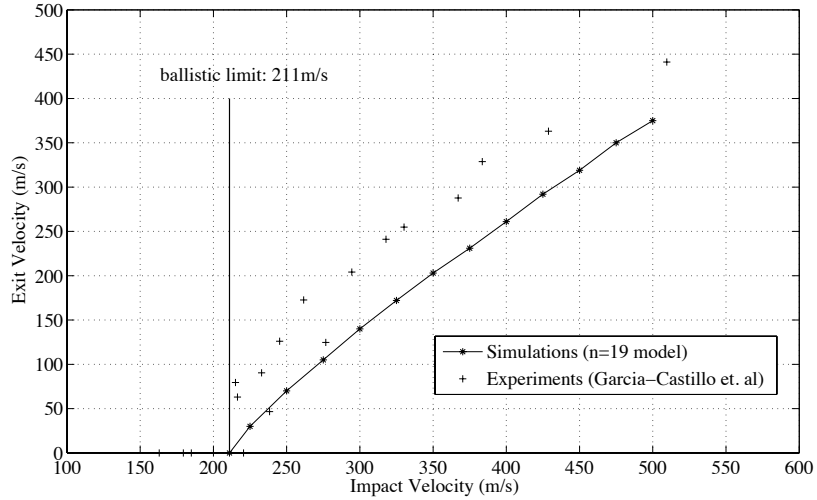

Figure 4.12. Variation of the exit velocity with respect to impact velocity.

According to [38], during the high velocity ballistic penetration of fiber reinforced polymer matrix composite targets, the main energy absorption mechanisms can be categorized as following.

- Cone formation and its growth at the back face of the target
- Failure of in-plane primary fibers
- Deformation of in-plane secondary fibers
- Delamination and matrix cracking
- Punching shear failure
- Friction between target and projectile during penetration

Within the deformation cone, fibers directly below the projectile are called as primary fibers and remaining fibers in the deformation cone are termed as secondary fibers. Primary fibers absorb energy by fiber breakage whereas energy in secondary fibers in absorbed by deformation.

According to [38], [39], In case of thin woven laminates, for impacts with projectile having speed below ballistic limit, the energy is mainly absorbed by delamination and matrix cracking/crushing, whereas when projectile hits the target with speed above ballistic limit, fiber failure and momentum transfer between the detached laminate piece (plug) and projectile are main energy absorption mechanisms. When a projectile with velocity slightly more than ballistic limit penetrates the target, breakage of primary fibers takes place and causes perforation [39]. Sudden breakage of primary fibers may create an impulsive action on projectile. In case of projectile with velocity considerably higher than ballistic limit, the projectile is in contact with the laminate for too little time for laminate to respond [39]. This might be the reason for initial non-linearity in experimental impact velocity - exit velocity curve, which is followed by a linear trend at velocities considerably higher than the ballistic limit.

However, since the proposed formulation does not differentiate between various energy absorbing mechanisms at different stages, the entire simulated impact velocity - exit velocity curve is linear.

Fig. 4.13 provides interphase damage regions for impact velocities of 211, 300, 400 and 500 m/s. The size of the interphase damage region is observed to have only a slight variation with respect to the impact velocity, which is in agreement with the experimental response.

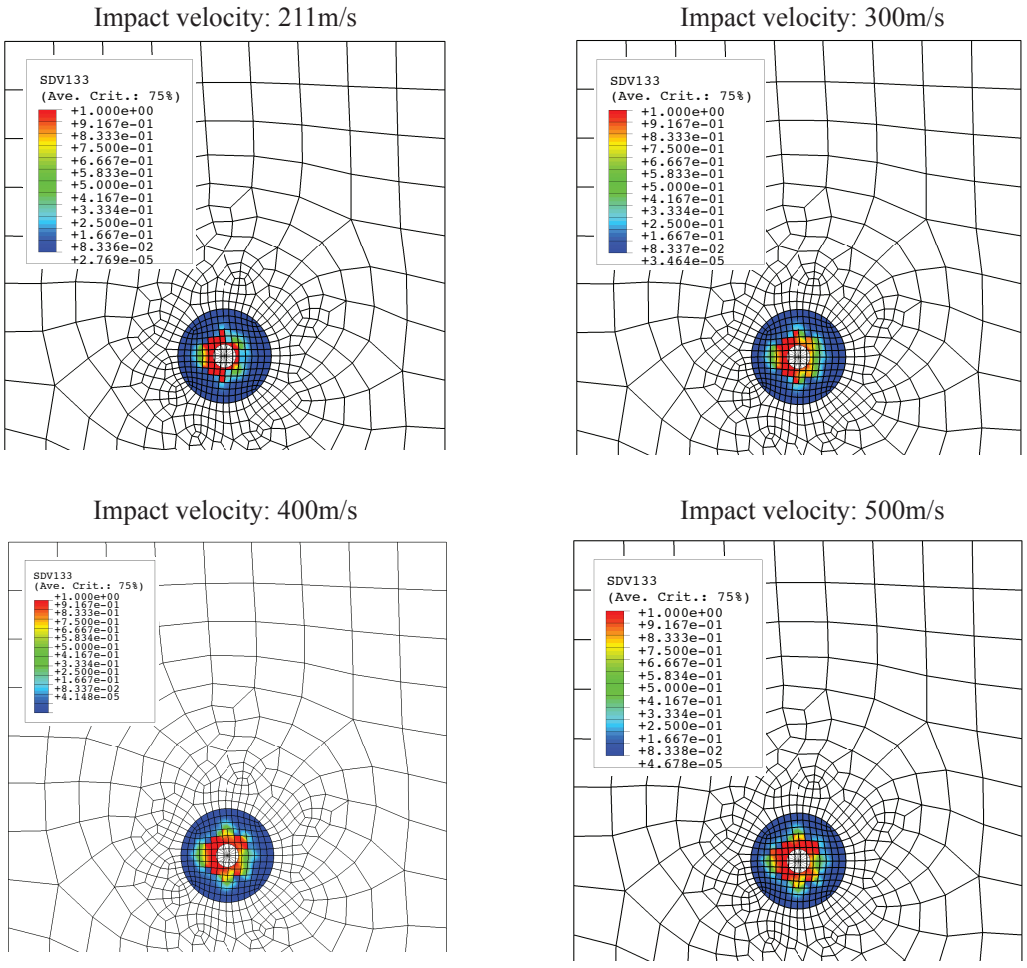

Figure 4.13. Interphase damage variation around the impact zone at impact velocities (a) 211 m/s, (b) 300m/s, (c) 400 m/s (d) 500 m/s.

CHAPTER V

CONCLUSIONS AND RECOMMENDATIONS

The proposed methodology successfully presents a multiscale framework for static and dynamic in-elastic analysis of thin heterogeneous plates. Reduced order homogenization makes it more computationally efficient in comparison with classical homogenization techniques. With the availability of sufficient experimental test results for model parameter determination, the successful association of the proposed methodology with the commercial finite element package, Abaqus, makes it directly useful for industrial sector. The inelastic portion of total strain has been dealt with the help of transformation field analysis which makes the entire non-linear problem easier to manage during formulation.

The problem of mesh dependence of macroscopic finite element solution has been successfully reduced with the help of viscous regularization, as shown in results of uniaxial tension tests (Fig. 4.9). Results of three point bend test (Fig. 4.4 and 4.5) agree well with the reference three dimensional solution at various loading rates. This exhibits the capabilities of the proposed methodology in successfully dealing with rate dependent problems. Successful simulation of ballistic limit (Fig. 4.12) and damage area (Fig. 4.13) in high velocity ballistic impact problem with respect to available experimental results presented in [36], presents another possible area of application of the proposed methodology.

The methodology presented in this manuscript deals only with small deformation thin plate problems. The extension of the proposed framework to accommodate large deformations for thin plates needs to be investigated within the framework of

eigendeformation and reduced order homogenization. Another area of improvement could be the extension of proposed framework to include the deformation modes of moderately thick and thick plates. The work presented here implements static partitioning strategy for unit cell segmentation. Although, this partitioning strategy works excellent here, other partitioning strategies, including dynamic strategies, proposed in [35] needs to be investigated.

REFERENCES

[1] Belytschko T., Hughes T J R, Patankar N, Herakovich C T and Bakis C E, Research directions in computational and composite mechanics, *A report to United States National Committee on Theoretical and Applied Mechanics,* , June 2007.

[2] Timoshenko S P and Goodier J N, *Theory of Elasticity* , McGraw-Hill, 1970.

[3] Reddy J N, *Mechanics of Laminated Plates and Shells: Theory and Analysis* , CRC Press, 1997.

[4] Carrera E, An Assessment if Mixed and Classical Theories on Global and Local response of Multilayered Orthotropic Plates, *Composite Structures* , 50, 183 - 198, 2000.

[5] Sanchez-Palencia E., *Homogenization Techniques for Composite Media: Lectures Delivered at the Cism International Center for Mechanical Sciences Udine, Italy, July 1-5, 19 (Lecture Notes in Physics)*, Springer - Verlog, 1987.

[6] manevitch L I, Andrianov I V and Oshmyan V G, *Mechanics of Periodically Heterogeneous Structures* , Springer, 2002.

[7] Caillarie D, Thin Elastic and Periodic Plates, *Mathematical Methods in The Applied Sciences* , 6, 159-191, 1984.

[8] Kohn R V and Vogelius M, A New Model for Thin Plates wth Rapidly Varying Thickness, *International Journal of Soilds and Structures* , 20(4), 333-350, 1984.

[9] Lewinski T, Effective Models of Composite Periodic Plates - I, Asymptotic Solution, *International Journal of Soilds and Structures* , 27(9), 1155 - 1172, 1991.

[10] Lewinski T, Effective Models of Composite Periodic Plates - II, Simplification Due to Symmetries, *International Journal of Soilds and Structures* , 27(9), 1173 - 1184, 1991.

[11] Lewinski T, Effective Models of Composite Periodic Plates - III, Two-dimensional Approaches, *International Journal of Soilds and Structures* , 27(9), 1185 - 1203, 1991.

[12] Lewinski T and Telega J J, *Plates, Laminates and Shells: Asymptotic Analysis and Homogeinzation* , World Scientific Press, 1999.

[13] Lammerant L and Verpoest I, Modelling of The Interaction Between Matrix Cracks and Delaminations During Impact of Composite Plates, *Composite Science and Technology* , 56, 11711178, 1996.

[14] Garg A C, Delamination A Damage Mode in Composite Structures, *Engineering Fracture Mechanics* , 29(2), 557 - 584, 1988.

[15] Godoy L A, Finite Element/Perturbation Analysis of Plates and Shells with Geometric Damage using a Sympbolic Manipulator, *International Journal of Pressure Vessel and Piping* , 73, 249 - 257, 1997.

[16] Voyiadjis G J and Deliktas B, A Coupled Anisotropic Damage Model for the Inelastic Response of Composite Materials, *Computer Methods in Applied Mechanics and Engineering* , 183, 159 - 199, 2000.

[17] Tay T E, Liu G, Tan V B C, Sun X S and Pham D C, Progressive Failure Analysis of Composites *Journal of Composite Materials* , 42, 1921 - 1966, 2008.

[18] Executive Summary, *International Journal of Solids and Structures* , 37, 1-11, 2000.

[19] Talreja R, A Continuum Mechanics Characterization of Damage in Composite Materials, *Proceedings of The Royal Society of London, Series A, Mathematical and Physical Sciences* , 399(1817), 195 - 216, 1985.

[20] Krajcinovic D, Damage Mechanics: Accomplishments, Trends and Needs, *International Journal of Solids and Structures* , 37, 267-277, 2000.

[21] Krajcinovic D, *Dmagae Mechanics*, Elsevier, 1996.

[22] Kachanov L M, *Introduction to Continuum Damage Mecchanics* , Martinus Nijhoff Publishers, 1986.

[23] Iannucci L and Ankersen J, An Energy Based Damage Model for Thin Laminated Composites, *Composite Sciecne and Technology* , 66, 934 - 951, 2006.

[24] Ladevere P, A Damage Computational Method for Composite Structures, Computers and Structures, 44(1 - 2), 79 - 87, 1992.

[25] Corigliano A, Formulation, Identification and Use of Interface Models In the Numerical Analysis of Composite Delamination, *International Journal of Solids and Structures* , 30(20), 2779 - 2811, 1993.

[26] Collombet F, Bonini J and Lataillade J L, A Three-dimensional Modelling of Low Velocity Impact Damage in Composite Laminates, *International Journal for. Numerical Methods in Engineering* , 39(9), 1491 - 1516, 1996.

[27] Dvorak G J and Benveniste Y, On transformation Strains and Uniform Fields in Multiple Elastic Media, *Proceedings of The Royal Society of London, Series A, Mathematical and Physical Sciences* , 437(1900), 291-310, 1992.

[28] Dvorak G J, Transformation Field Analysis of Inelastic Composite Materials, *Proceedings of The Royal Society of London, Series A, Mathematical and Physical Sciences* , 437(1900), 311-327, 1992.

[29] Oskay C and Fish J, Eigendeformation-Based Reduced Order Homogenization for Failure Analysis of Heterogenoeus Materials, *Computer Methods in Applied Mechanics and Engineering* , 196(7), 1216-1243, 2007.

[30] Geers M G D and Brekelmans W A M, Viscous Redularization of Strain-Localization for Damaging Materials, *DIANA Computational Mechanics '94, Eds: Kusters G M A and Hendriks M A N, Kluwer Academic Publishers* , 127 - 138, 1994.

[31] Needleman A, Material Rate Dependence and Mesh Sensitivity in Localization Problems, *Computer Methods in Applied Mechanics and Engineering* , 67, 69-96, 1988.

[32] Simo J C and Ju J W, Strain- and Stress-based continuum damage models - I. Formulation, *International Journal of Solids and Structures* , 23(7), 821-840, 1987.

[33] Riley K F, Hobson M P and Bence S J, *Mathematical Methods for Physics and Engineering* , Cambridge Univeristy Press, 2006.

[34] COurant R and Hilbert D, *Methods of Mathematical Physics (E-book, Accesible through Vanderbilt University Library)* , WIley Publishers, 1989.

[35] Oskay C and Pal G, A multiscale model for analysis of thin heterogeneous plates, *Journal of Damage Mechanics, Special Issue on Multiscale Damage and Failure Mechanics* , Submitted.

[36] Garcia-Castillo S K, Sanchez-Saez S, Barbero E and Navarro C, Response of Pre-Loaded Laminate Composite Plates Subject to High Velocity Impact, *Journal de Physique IV* , 136, 1257-1263, 2006.

[37] Oskay C and Fish J, On Calibration and Validation of Eigendeformation-based Multiscale Models for Failure Analysis of Heterogeneous Materials, *Computational Mechanics*, 42(2), 181-195, 2008.

[38] Naik N C, Shrirao P and Reddy B C K, Ballistic Impact Behavior of Woven Fabric Composites: Formulation, *International Journal of Impact Engineering* , 32, 1521 - 1552, 2006.

[39] Lopez-Puente J, Zaera R and Navarro C, Experimental and Numerical Analysis of Normal and Oblique Ballistic Impacts on Thin Carbon/Epoxy Woven Laminates, *Composites: Part A* , 39, 374 - 387, 2008.